Acceleration and trapping of fast ions in self-organized magneto-plasma structures in the dense plasma focus

S. K. H. Auluck (iD)

View Online   Export Citation   CrossMark

ARTICLES YOU MAY BE INTERESTED IN

Acceleration and trapping of fast ions in self-organized magneto-plasma structures in the dense plasma focus

S. K. H. Auluck[a] (iD)

AFFILIATIONS

International Scientific Committee for Dense Magnetized Plasmas, Hery 23, P.O. Box 49, 00-908 Warsaw, Poland

[a]Author to whom correspondence should be addressed: skhauluck@gmail.com. URL: http://www.icdmp.pl/isc-dmp

ABSTRACT

Recent research at the PF-1000 Dense Plasma Focus facility strongly suggests that the early part of neutron emission is caused by fast deuterons with energy on the order of $\sim$100 keV, having approximately equal axial and radial velocity, temporally coinciding with the occurrence of self-organized, bounded magneto-plasma structures, which remain trapped within the reaction zone for tens of transit times. The experimental evidence, predominantly qualitative in nature, does not clarify the nature and origin of the accelerating electric field responsible for high ion energy and of the magnetic field that might be confining the ions to the reaction zone except for the suggestion that they have toroidal and poloidal magnetic field components whose presence is revealed by magnetic probes. Current theories, conjectures, and models of plasma focus find it difficult to accommodate three-dimensional features of ion motion and magnetic field revealed by multiple experiments within their scope. This paper revisits the relevant experimental evidence and introduces a model that is deliberately non-quantitative in order to accommodate the qualitative nature of the available experimental evidence. The model leads to a functional form for the 3-dimensional distribution of magnetic field associated with the spontaneously self-organized magneto-plasma structures. This enables the discussion of properties of 3-dimensional trajectories of ions accelerated by electric fields induced during their growth. Many qualitative observations about the nature of neutron emission in Dense Plasma Focus and the observed phenomenology of plasma evolution can be understood in terms of this model in a unified manner. The model also helps conceive a new generation of diagnostic schemes targeted at getting quantitative information that is out of reach of currently available diagnostics.

Published under license by AIP Publishing. https://doi.org/10.1063/1.5139609

NOMENCLATURE

COB	complete orthonormal basis
CCW	counterclockwise
CW	clockwise
DPF	dense plasma focus
CK	Chandrasekhar–Kendall
CM	center of mass
GEM	gas electron multiplication
HXR	hard X rays
ICCD	intensified charge coupled device
LHS	left hand side
MHD	magneto hydro dynamics
PPW	poloidal potential well
QS	quasi-stationary
RGV	resistive Gratton-Vargas
SAD	spectral amplitude density
SSS	spontaneously self-organized state
SSNTD	solid state nuclear track detector
T-mode	transient mode
ToF	time of flight
μCAD	micro-collimator-array-detector

I. INTRODUCTION

Dense Plasma Focus (DPF)[1–4] is a laboratory fusion device well known for its fourth-power-of-current scaling of neutron yield and many mysterious properties of its neutron emission[5,6] which include the following:

- The fusion reaction rate is at least two orders of magnitude more than estimates based on thermonuclear reaction rate at ion

temperature and plasma density measured using Thomson scattering.[7]

- There is unmistakable evidence[8–11] from neutron Time-of-Flight (ToF) spectroscopy that the center of mass (CM) of deuterons participating in fusion reactions moves along the direction of current with CM kinetic energy on the order of 100 keV—there is a noticeable shift of the peak of neutron spectra toward higher energy in the direction of current.

- The interpretation of this shift in terms of a *linear* beam presumably accelerated in a "virtual plasma diode"[12] created by the m = 0 pinching instability is negated by evidence for the existence of equally fast ions in the direction opposite to the current[13–15] and by evidence that the neutron emission begins well before the instability.[16]

- Time-resolved neutron anisotropy studies on POSEIDON reveal[16] that the first pulse of neutrons has fluence anisotropy less than unity indicating that "accelerated ions move predominantly perpendicularly to the pinch axis."[16]

- Side-on neutron ToF measurements[17] at the Frascati 1 MJ plasma focus reported "a 100 keV deuteron loop in the plane determined by the gun axis and the observational direction"

- There is a report[18] from Frascati describing "evidence of a 100 keV d+ stream orbiting in a plane perpendicular to the experiment main axis." Rotational motion of CM of reacting deuterons about the axis is also inferred from the POSEIDON plasma focus at Stuttgart[19] where space-resolved time-integrated fusion proton spectroscopy exhibits lateral energy asymmetry.[5] *These reports imply that the ion trajectories have dimensions comparable with the dimensions of the hot and dense plasma seen by imaging techniques.*

- The duration of neutron emission is much larger than the transit time of deuterons having energy ∼100 keV across dimensions of the plasma column.[10–12,14] This fact can be reconciled with the particle and energy content available within the plasma only by the assumption that the fast deuterons move along trajectories that are bounded within dimensions comparable with the dimensions of the plasma,[18–20] making the ions traverse the same region repeatedly. The possibility that neutron emission signal is broadened because of scattering or because of reactions occurring in the neutral gas above the pinch has been discounted in POSEIDON and Frascati by shielding the neutron detectors with a water tank and by placing an obstacle above the pinch, respectively.

- There are at least two reports which affirm that in some shots, the plasma column did not break up due to instability and still the neutron yield was unaffected, *indicating that instabilities do not form a necessary part of DPF physics.* The Frascati plasma focus had a high pressure, neutron-optimized mode of operation[20] where the plasma column was "totally MHD-quiescent." In the PLAMYA plasma focus,[21] MHD instabilities were reported to be a rare event.

- Fusion reaction zone localization studies on POSEIDON using a time-resolved 1-dimensional neutron pinhole camera technique[16] showed that during the first pulse, the neutron source had an axial size limited to 6.5 cm, similar to the height of the plasma stem seen in Schlieren pictures. On the other hand, 3-dimensional time-integrated reconstruction of the fusion proton source[16] showed an axial extension of roughly 9 cm and a

diameter of about 6 cm, much more than the diameter of the plasma as seen in Schlieren pictures.[16] Similar conclusions were reported earlier from Frascati 1 MJ plasma focus.[20]

- Neutron emission begins well before the characteristic current derivative singularity in POSEIDON[22] and maximum plasma compression, clearly indicating that phenomena associated with the instability of the plasma column are not the primary cause of the neutron emission.

At present, there exists no theoretical construct that can explain all the above aspects of neutron emission in a unified manner. The present paper aims to explore a theoretical approach that has the potential to perform that difficult task.

So far, attempts to explain these features have been centered about the hypothesis that fast ions are somehow generated and trapped in large gyroradius orbits that encompass the device axis. Specifically interesting is the report from POSEIDON[19,22,23] that compares experimental time-integrated reaction proton spectra with an ion-optic model (Gyrating Particle Model) that concludes that (a) the first neutron pulse that precedes the m = 0 instability has intensity ∼500 times higher than thermal estimates, (b) has very low fluence anisotropy, (c) has a "macroscopically quiet outer boundary," and (d) has no micro-turbulence. It claims the existence of an accelerating mechanism in the pinch phase that accelerates ions up to 400 keV with a power-law energy distribution. The model is consistent with the hypothesis of trapping of ions up to 100 ns "by gyromotion and relaxation," which is also the duration of the first pulse of neutrons.

Such 3-dimensional gyromotion of ions in trajectories of dimensions comparable to plasma size is not possible[12] unless the associated magnetic field itself has a 3-dimesional structure of size comparable to the plasma size. A clear signature of existence of axial magnetic field in the pinch phase over scale length comparable with the pinch was found in the tilt of reaction proton image with respect to the neutron image in POSEIDON data.[22] The Gyrating Particle Model calculations indicated that the *observed tilt could be reproduced only if an azimuthal current of 400 kA was assumed to exist on the periphery of the pinch column.*[22] Existence of axial magnetic field in the plasma focus has been reported by other laboratories as well.[5]

Correlation between three-frame Schlieren diagnostics and neutron pinhole camera diagnostics at Frascati[20,24] suggests that "long-lasting plasma blobs whose decay time (100–150 ns) corresponds to that of the local neutron emission" also have radial and axial dimensions which correspond strongly to the dimensions of the neutron source. Similar plasma blobs have been observed using soft x-ray pinhole diagnostics in the Nessi plasma focus.[25]

Recent research at the PF-1000 Dense Plasma Focus at the International Center for Dense Magnetized Plasmas, Warsaw, Poland has generated the following evidence that supports the view that presence of trapped accelerated ions is closely related to emergence of spontaneously self-organized, bounded magneto-plasma structures (generically called as "plasmoids"[26])

- The plasmoid structure formed by transport of plasma from the boundary to the inner layers as visualized in 15-frame time-resolved interferometry coincides in time with soft and hard x-ray and neutron emission.[27,28]

- Magnetic probes confirm the existence of axial magnetic field in the pinch region[29] and its temporal correlation with neutron

emission[29,30] as well as with formation and decay of plasmoidal structures.

- A dense structure with a radius of 2 cm is formed at the end of implosion,[31] whose deuteron content remains constant during the neutron production.

- Reaction proton images show that the reaction zone is larger than the dense plasma zone.[31]

- The first part of neutron emission that begins few tens of nanoseconds before the current derivative singularity coincides with the stagnation phase, precedes the breakup of plasma column, and has negligible energy anisotropy[32] indicating that the fast deuterons producing those neutrons had similar radial and axial velocity components with energy on the order of $\sim$100 keV.[33,34]

- There is evidence[35] for the existence of a return current path outside the dense pinch column, with toroidal and poloidal components. This represents a distribution of closed loops of sheared current density,[36] which enclose a low density "bubble" plasma. The return current is directed in opposite sense to the main discharge current connecting a pair of symmetrical protrusions (termed "lobules"[36]) along the boundary of the plasma column or one lobule and the anode. The main discharge current flows beyond this return path. A similar phenomenon was also reported from Frascati 1 MJ focus.[20]

- There is evidence for existence of localized sources of fast ions in regions of plasma external to the dense pinch.[36]

- Using XUV spectroscopy of impurity lines, electron and ion temperatures are estimated[33] to be about 70 eV at the end of stagnation phase which coincides with the beginning of the spontaneous self-organization phase. Electron thermal transit time across plasma dimensions $\sim$1 cm can, therefore, be estimated to be about 3 ns. The transit time of a 200 keV deuteron across 1 cm is also $\sim$2 ns while the duration of neutron emission is $\sim$100–150 ns. The estimates of plasma density[33] using Abel inversion on interferometric fringes are in the region of 10^{24}–10^{25} electrons/m^3. The magnetic field in the plasmoid is estimated as being on the order of $\sim$10 T both from local hydromagnetic equilibrium considerations and from probe measurements.[33] The Larmor radius of 200 keV deuteron in 10 T magnetic field is $\sim$0.9 cm which is comparable with plasma dimensions. The Alfven velocity for these parameters evaluates to $\sim$1.5 $\times$ 10^5 m/s and the Alfven transit time across plasma dimension $\sim$1 cm is $\sim$65 ns. In comparison, the duration of the laser pulse used in interferometry is less than 1 ns[33] and the inter-frame separation is $\sim$10–20 ns. The conclusion is that the interferometer system is capable of capturing plasma dynamics information at the time scale of ion acceleration which occurs also on the time scale of electron thermal redistribution. Significant plasma reconfiguration occurs at the Alfven velocity over the duration of the neutron emission. Scale length of the plasma reconfiguration closely matches the estimated gyroradius of accelerated deuterons responsible for neutron emission.

Extensively studied[27–36] topological transformations occurring in PF-1000 suggest[35,36] that the acceleration of charged particles in the DPF can be a result of magnetic reconnection.[37,38] Magnetic reconnection—defined[37] as "topological rearrangement of the magnetic field in a plasma on a time scale faster than allowed by microscopic forms of dissipation"—itself is a vast field being actively researched

both in connection with astrophysics and magnetically confined fusion.[37,38] Such topological reconfiguration requires the breaking of the "frozen magnetic flux constraint" of ideal magnetohydrodynamics (MHD).[41] Among the issues being actively researched[37,38] but not yet fully understood are the following: (1) "fast reconnection"—the apparent independence of the speed of reconnection from the magnitude of terms that violate the frozen magnetic flux constraint of ideal MHD model; (2) "trigger"—the sharp transition between a relatively slow energy accumulation stage and a rapid energy release stage; (3) "energy conversion modes:" the manner in which the energy release is converted into electron and ion heating, generation of fast particles and bulk plasma flow; (4) "multiple spatial scale effects:" energy stored on the global scale length is released because of non-ideal-MHD phenomena that occur at characteristic microscopic scale lengths for electrons and ions such as collisional mean free paths, collisionless skin depths, gyroradii, etc., *indicating that interaction between phenomena occurring on vastly differing spatial scales cannot be neglected*, introducing a major difficulty in the theoretical study of reconnection.

This difficulty can be mitigated to some extent in the study of one particular aspect of magnetic reconnection—the spontaneous self-organization of plasma and magnetic field together (sometimes termed as "magneto-plasma"). Spontaneous self-organization is an important manifestation of the global scale effects of magnetic reconnection,[38] where a global MHD equilibrium configuration can lower its total energy by undergoing a change in its topology. Certain volume integrals of quadratic forms involving plasma vector fields can be shown to be invariant in the limit of vanishing dissipation in a class of fluid models of plasma. The interplay of multiple spatial scales is reflected in the emergence of a hierarchy of time scales of such quadratic invariants in the presence of dissipation, usually in an incompressible flow regime. Minimization of the fastest decreasing invariant in the presence of dissipation, holding the rest of the invariants constant, leads to a variational problem whose solution can be considered to be the spontaneously self-organized state on an intermediate time scale longer than that of the fastest decreasing invariant but smaller than the timescales of the remaining invariants. This approach has been investigated extensively with many variations on the basic theme. Taylor[39] has minimized magnetic energy keeping magnetic helicity constant. Sudan[40] has minimized the sum of kinetic, magnetic, and thermal energies keeping 3-components of canonical momenta, magnetic helicity, and total mass constant. Turner[41] and Steinhauer and Ishida[42] have minimized the sum of magnetic and kinetic energy keeping the magnetic helicity and hybrid helicity constant. Yoshida and Mahajan[43] minimize the squared modulus of the generalized enstrophy (curl of the canonical momentum) while keeping energy, magnetic helicity, and helicity of generalized vorticity constant. Dasgupta *et al.*[44] minimize the Ohmic energy dissipation rate keeping the magnetic helicity constant. Khalzov *et al.*[45] minimize energy using axial magnetic flux, axial momentum, angular momentum, magnetic helicity, and cross helicity as constants. The minimum energy state is usually expressed as a linear combination of curl eigenfunctions, also known as Chandrasekhar-Kendall (CK) functions[46] and generalized Beltrami states.[43] Thus Taylor's relaxed state[39] consists of a single CK function. Relaxed state in the theories of Turner,[41] Steinhauer and Ishida,[42] and Yoshida and Mahajan[43] consists of two CK functions. That of Dasgupta *et al.*[44] consists of three CK functions. A generalization[47] of the relaxation theory of Yoshida and Mahajan[43] for an N-species

plasma produces a relaxed state of N CK functions all with distinct eigenvalues.

There are two fundamental obstacles to extending the insights from such relaxation models to the case of DPF. The first obstacle is that these models are developed in the context of specific plasma devices, which have a conducting boundary close to the plasma while the DPF has no "close-in" conducting boundaries (it shares this feature with astrophysical plasmas). The second obstacle is that all those devices have an externally injected magnetic flux whose magnitude is an experimental control parameter, while the DPF has no externally applied magnetic flux except that from Earth's magnetic field.[6] Both these circumstances find a prominent place in the theoretical developments of the relaxation models—the first in specifying strict boundary conditions on the plasma model and the second in determining the unknown parameters of the theoretical development and in providing a dynamo mechanism. The suggested similarity[36] between spheromaks formed in a coaxial gun and plasmoidal structure in DPF does not take into account these crucial differences.

However, the evidentiary linkage of neutron emission and associated fast charged particles in DPF with spontaneous topological transformations of the 3-dimensional plasma and magnetic field structure is a very significant advance and the basis of the conjecture[35] that fast ions responsible for fusion neutrons in a DPF are produced as a result of magnetic reconnection. To use this experimental information to explain the properties of neutron emission enumerated above requires a model of not just generation of fast particles but also their confinement in bounded trajectories of size comparable with the plasma. Such model must necessarily provide conceptualization of 3-dimensional structure for electric and magnetic field for acceleration and confinement of ions, but while doing so, cannot utilize the considerable work done on magnetic reconnection and plasma relaxation for the reasons explained above. Keeping in view the qualitative nature of conclusions from experimental data, the model should aim to produce matching qualitative conclusions. This paper aims to outline such model.

The point of departure for this model is the mathematical result[48] that Chandrasekhar-Kendall functions[46] (eigenfunctions of curl) in cylindrical geometry defined over infinite domain, their generating functions (eigenfunctions of the Laplacian with negative eigenvalues), and gradients of the latter are orthogonal complete sets of basis functions for solenoidal fields, scalar fields, and irrotational fields, respectively. As a result, any model of plasma (for example single fluid, two fluid, four fluid,[22] ideal MHD, Hall MHD, resistive MHD, etc) that can be expressed in terms of solenoidal, scalar and irrotational fields in space can be transformed into a set of temporal evolution equations in the corresponding mode number space. Differential operators in such models act on the basis functions and are reduced to algebraic expressions involving mode numbers. Stochastic fields can be incorporated[48] in the model to represent random electromagnetic fields from radiation or turbulence. Nonlinear terms in the model equations give rise to terms in the transform space which couple mode numbers generating *evolution of modes at sum and difference of the coupled mode numbers.*[49]

The net result of such exercise would be to transport Spectral Amplitude Density (SAD) of each physical field in mode number space from its initial distribution, prescribed by plasma formation and evolution dynamics, to another one, where SAD concentrates at the lower and higher ends of the mode number spectrum. This should occur without recourse to any special boundary conditions or without

being limited to any specific plasma model, which are a common feature of all relaxation theories. Physical effects place limits on the smallest and highest mode numbers that can be reached during the course of such evolution. The finite size of the plasma resulting from its global dynamics puts a lower bound on the mode numbers and microscopic effects place an upper bound on the mode numbers. As a result, the plasma appears to spontaneously self-organize into a "double-Beltrami" state—a linear combination of two curl eigenfunctions with scale lengths, which are reciprocal eigenvalues, on the order of the plasma size and on the order of a microscopic scale length. A two-species plasma with Hall effect has[41] a characteristic scale length on the order of the collisionless ion skin depth c/ω_{pi}. There is experimental evidence that filamentary structures in a small plasma focus have a scale length of the order of $c/\omega_{pi} \sim 0.1$ mm.[50] There is also experimental evidence of sub-millimeter size structures in DPF using gated Intensified Charge Coupled Device (ICCD) camera,[51] soft-x-ray images,[23,52,53] and ion pinhole camera.[52] Observations of a complex structure of interweaving filaments forming "magnetic flux ropes"[54] and "dynamic percolating network"[55] in plasma focus along with a "spheromak-like" structure also support the idea that the SAD condenses at the extreme ends of the mode number space.

The rationale for this approach is that it leads to a mathematical form—the curl eigenfunction—for the expected 3-dimensional structure of magnetic field of the spontaneous self-organized state observed in DPF which has no well-defined "close-in" boundary that can satisfy the exact boundary conditions required by most theories of spontaneous self-organization in plasmas. The turbulent cascade should induce electric and magnetic fields with a wide spectrum of space and time scales, perhaps with some in-built randomness. Ions should be accelerated under the influence of such electric field and deflected by the magnetic field resulting in trajectories that could remain bounded within a compact spatial region comparable in size with the plasma under appropriate conditions. This paper investigates the properties of such ion trajectories and shows that many aspects of the neutron emission data can be explained in terms of these properties.

Section II introduces the mathematical basis of the model. Section III sets out the model assumptions concerning the structure of the spontaneously self-organized state (SSS) and derives the main results concerning the existence and disposition of bounded ion orbits in relation to SSS. Section IV discusses feasible, untried diagnostic schemes for generating quantitative data that can be used to refine the model in a quantitative manner. Section V concludes the paper by summarizing its main findings.

II. SPATIAL STRUCTURE OF SPONTANEOUSLY SELF-ORGANIZED MAGNETIC FIELD

Self-organization in plasmas is usually studied in the context of plasma devices which have a close-in metallic boundary, which allows construction of theories with special boundary conditions on magnetic and velocity fields which assert *vanishing* of certain field components on the boundary—a very stringent requirement. The application or extension of such theories to the case of DPF encounters a basic obstacle: the absence of a close-in boundary and consequent inability to prescribe "hard" boundary conditions for magnetic, velocity or density/pressure fields. Consequently, the neat analytical expressions[37–43] that are used to describe the spontaneous self-organization in conventional magnetic confinement fusion devices seem to be out of reach of DPF

physics. This section, therefore, is devoted to developing an argument that can yield an analytical handle on spontaneous self-organization in the DPF in spite of the absence of close-in metallic boundaries.

The starting point of the discussion is the following mathematical result related to eigenfunctions $\vec{\chi}$ of the curl (Chandrasekhar–Kendall modes[46])

$$\vec{\nabla} \times \vec{\chi} = sk\vec{\chi}, \ s = \pm 1, \quad 0 \leq k \leq \infty, \tag{1}$$

which can be expressed in terms of eigenfunctions ψ of the Laplacian (Helmholtz modes)

$$\nabla^2 \psi = -k^2 \psi \tag{2}$$

by the relation[46]

$$\vec{\chi} = sk^{-1}\vec{\nabla} \times \vec{\nabla} \times (\psi \hat{z}) + \vec{\nabla} \times (\psi \hat{z}), \tag{3}$$

where the first term is the poloidal component and the second is the toroidal component. In simply connected cylindrical domains with periodic boundary conditions along the axis, ψ and $\vec{\chi}$ are expressed by the relation

$$\psi_{m\kappa\gamma} = J_m(\gamma r)\exp(im\theta - i\kappa z), \tag{4}$$

$$\vec{\chi}_{m\kappa\gamma s}(r,\theta,z) = k^{-2}\exp(im\theta - i\kappa z)$$
$$\times \begin{pmatrix} i\frac{1}{2}\gamma\hat{r}\left((sk+\kappa)J_{m+1}(\gamma r) + (sk-\kappa)J_{m-1}(\gamma r)\right) \\ +\frac{1}{2}\gamma\hat{\theta}\left((sk+\kappa)J_{m+1}(\gamma r) - (sk-\kappa)J_{m-1}(\gamma r)\right) \\ +\hat{z}\gamma^2 J_m(\gamma r) \end{pmatrix}. \tag{5}$$

The radial mode number γ and axial mode number κ are related to the magnitude of eigenvalue k by the relation $\gamma = \sqrt{k^2 - \kappa^2}$. Right and left handed helical modes are represented by the handedness index $s = \pm 1$.

It can be shown that, over simply connected infinite cylindrical domain, $\vec{\chi}_{m\kappa\gamma s}$, $\psi_{m\kappa\gamma}$, and $k^{-1}\vec{\nabla}\psi_{m\kappa\gamma}$ form the orthogonal complete sets of *dimensionless* basis functions for solenoidal fields, scalar fields, and irrotational fields respectively, as expressed by the following identities:[46]

$$\int d^3\vec{r}\,\vec{\chi}^*_{m\kappa\gamma s} \cdot \vec{\chi}_{m'\kappa'\gamma's'} = 8\pi^2 k^{-2}\gamma\delta_{mm'}\delta_{ss'}\delta(\kappa'-\kappa)\delta(\gamma'-\gamma), \tag{6}$$

$$\int d^3\vec{r}\,\psi^*_{m\kappa\gamma}\psi_{m'\kappa'\gamma'} = 4\pi^2\gamma^{-1}\delta_{mm'}\delta(\kappa'-\kappa)\delta(\gamma'-\gamma), \tag{7}$$

$$\int d^3\vec{r}\,\vec{\nabla}\psi^*_{m\kappa\gamma} \cdot \vec{\nabla}\psi_{m'\kappa'\gamma'} = 4\pi^2 k^2\gamma^{-1}\delta_{m,m'}\delta(\kappa-\kappa')\delta(\gamma-\gamma'), \tag{8}$$

$$\int d^3\vec{r}\,\vec{\nabla}\psi^*_{m\kappa\gamma} \cdot \vec{\chi}_{m'\kappa'\gamma's'}$$
$$= 4\pi^2 ik^{-2}\delta_{m,m'}\left\{\kappa\gamma' - \gamma\kappa'\right\}\delta(\kappa'-\kappa)\delta(\gamma'-\gamma) = 0$$
$$\int d^3\vec{r}\,\vec{\nabla}\psi_{m\kappa\gamma} \cdot \vec{\chi}_{m'\kappa'\gamma's'}$$
$$= -i4\pi^2(-1)^m\delta_{m,-m'}k^{-2}\left\{\gamma\kappa' + \kappa\gamma'\right\}\delta(\kappa'+\kappa)\delta(\gamma-\gamma') = 0. \tag{9}$$

For all solenoidal fields $\vec{F}_{SOL}(\vec{r},t)$, irrotational fields $\vec{F}_{IR}(\vec{r},t)$, and scalar fields $S(\vec{r},t)$, where $\vec{r}$ is the position vector, the following transform

relations hold without invoking any special boundary conditions (other than the conditions for existence of the integrals):

$$\vec{F}_{SOL}(r,\theta,z,t) = \sum_{s'}\sum_{m'=-\infty}^{\infty}\int_{-\infty}^{\infty}d\kappa'\int_0^{\infty}d\gamma'\,\mathscr{F}^{SOL}_{m's'}(\kappa',\gamma',t)\vec{\chi}_{m'\kappa'\gamma's'}(r,\theta,z),$$

$$\mathscr{F}^{SOL}_{ms}(\kappa,\gamma,t) = \frac{k^2}{8\pi^2\gamma}\int_0^{2\pi}d\theta\int_{-\infty}^{\infty}dz\int_0^{\infty}rdr\,\vec{\chi}^*_{m\kappa\gamma s}(r,\theta,z)\cdot\vec{F}_{SOL}(r,\theta,z,t), \tag{10}$$

$$\vec{F}_{IR}(r,\theta,z,t) = \sum_{m'=-\infty}^{\infty}\int_{-\infty}^{\infty}d\kappa'\int_0^{\infty}d\gamma'\,\mathscr{F}^{IR}_{m'}(\kappa',\gamma',t)k'^{-1}\vec{\nabla}\psi_{m'\kappa'\gamma'}(r,\theta,z),$$

$$\mathscr{F}^{IR}_m(\kappa,\gamma,t) = \frac{\gamma}{4\pi^2 k}\int_0^{2\pi}d\theta\int_{-\infty}^{\infty}dz\int_0^{\infty}rdr\,\vec{\nabla}\psi^*_{m\kappa\gamma}(r,\theta,z)\cdot\vec{F}_{IR}(r,\theta,z,t), \tag{11}$$

$$S(r,\theta,z,t) = \sum_{m'=-\infty}^{\infty}\int_{-\infty}^{\infty}d\kappa'\int_0^{\infty}d\gamma'\,S_{m'}(\kappa',\gamma',t)\psi_{m'\kappa'\gamma'}(r,\theta,z),$$

$$S_m(\kappa,\gamma,t) = \frac{\gamma}{4\pi^2}\int_0^{2\pi}d\theta\int_{-\infty}^{\infty}dz\int_0^{\infty}rdr\,\psi^*_{m\kappa\gamma}(r,\theta,z)S(r,\theta,z,t). \tag{12}$$

These are mathematical identities without reference to the physical problems they might represent.

Any physical model that can be expressed in terms of solenoidal, irrotational, and scalar fields and their integer-order time and space differential operators can then be transformed into evolution equations in mode number space using identities (10)–(12), where the spatial differential operators act on the basis functions and generate algebraic expressions containing mode numbers. Such evolution equations express[48] the rate of change of spectral amplitude density of a mode represented by unprimed mode numbers (m, κ, γ, s) in terms of summations and integrations over algebraic expressions involving spectral amplitudes of mutually interacting primed $(m', \kappa', \gamma', s')$ and doubly primed $(m'', \kappa'', \gamma'', s'')$ mode numbers in a system of coupled ordinary differential equations. Nonlinear terms in such models contribute terms[48] that contain the factor $\delta_{m,(m'+m'')}\delta(\kappa' + \kappa'' - \kappa)$ as well as integrals over a product of three Bessel functions of the form

$$D^{\gamma\gamma'\ \gamma''}_{mm'm''} \equiv \int_0^{\infty}rdr J_m(\gamma r)J_{m'}(\gamma' r)J_{m''}(\gamma'' r). \tag{13}$$

An examination of this integral reveals[49] that it is approximated in the sense of distributions by the expression

$$D^{\gamma\gamma'\ \gamma''}_{mm'(m-m')}$$
$$\cong \frac{1}{2\sqrt{\gamma\gamma'}}\begin{Bmatrix} \delta(\gamma'' - (\gamma-\gamma'))H(\gamma-\gamma') \\ +(-1)^{m-m'}\delta(\gamma'' - (\gamma'-\gamma))H(\gamma'-\gamma) \\ +(-1)^{m'}\delta(\gamma'' - (\gamma'+\gamma)) \end{Bmatrix}, \begin{matrix} H(x) = 1 \ x \geq 0 \\ = 0 \ x < 0 \end{matrix}. \tag{14}$$

A method of incorporating in such models random electromagnetic fields arising out of radiation or turbulence is also illustrated.[48]

The resulting theoretical structure has the character of a mean-field theory: non-random components of fields have source terms quadratic in the amplitude of random field components and the random field amplitudes are governed by linear equations whose coefficients are functions of non-random components—a situation where spontaneous phase transitions are likely to occur depending on model details.

The net effect of the nonlinear terms is the *continuous evolution* of spectral amplitude density toward higher (sum of coupled mode numbers) and lower (difference of coupled mode numbers) mode numbers starting from a spectral distribution prescribed by initial and boundary conditions of the particular physical problem. As a result, the spectral amplitude density (SAD) of each field tends to condense at the higher and lower ends of the mode number space subject to physical constraints. The physical size of the plasma, governed by global dynamics, prescribes the lower limits of the radial and axial mode numbers. The physical model of the plasma prescribes the upper limit of the mode number, for example, the Hall MHD model has a characteristic scale length c/ω_{pi} which is seen[50] to correspond to the radius of filamentary structures in a small DPF. The spontaneous emergence of a self-organized state is thus conjectured to be the result of a turbulent cascade condensing SAD into eigenmodes of the respective field at the physical spatial scale of the plasma. This can happen, under appropriate conditions, in a phase-transition-like manner as mentioned above.[48]

Such turbulent cascade is the *expected* result of stagnation of the radially imploding plasma sheath near the axis. The kinetic energy and momentum associated with the radial velocity must be conserved even though the plasma is unable to continue its radial motion. In a purely hydrodynamic and ideally symmetric situation, this leads to a spike in the pressure at the axis followed by a reflected shock wave. In a strongly ionized and magnetized supersonic plasma with imperfect symmetry (caused by the presence[6] of Earth's magnetic field and Coriolis effect due to Earth's rotation which break symmetry with respect to orientation along the axis and azimuth), the radial momentum of ions and electrons is convected[56] in transverse directions giving rise to ion and electron vorticity (and kinetic and magnetic energy associated with vortex-like motion of ions and electrons), resulting in formation of vortex cells, which are described mathematically by the CK function decomposition.

Since spectral evolution in mode number space occurs through sum and difference between mode numbers of interacting modes, it is reasonable to expect that the spectrum would comprise integer multiples of mode numbers of a "fundamental mode" that can be related to the gross plasma dimensions governed by global dynamics of the DPF in a unique manner.

The Resistive Gratton-Vargas (RGV) model[57] provides a basis for estimating the fraction of stored energy converted into work done in accelerating the plasma, which can be assumed to determine the order of magnitude of the total energy content in the vortex spectrum. It also simulates the umbrella-like shape of the plasma. This shape, partially resembling a toroidal surface, is a common feature of DPF devices and can be taken to provide the reference for the "fundamental mode."

The above argument provides the basis for the model assumption that the spontaneous self-organized state (SSS) can be represented by a discrete spectrum of curl eigenfunctions consisting of low spatial harmonics of a fundamental mode with spatial scale length comparable with the dimensions of the plasma. It coexists with another superposition of curl eigenfunctions with scale length $\sim c/\omega_{pi}$ and its integer multiples. Since the two scale lengths differ by orders of magnitudes, they can be effectively treated as independent entities, although they have a common origin.

The fact that the laser pulse duration of the interferometry system on PF-1000 is less than the estimated electron transit time and the framing interval is less than the estimated Alfvén transit time across macroscopic plasma dimensions implies that the interferometry system is looking at the temporal evolution of mode spectrum under turbulent cascade conditions created by the stagnation of plasma at the axis.

III. MODELING AND CHARACTERIZATION OF ION TRAJECTORIES

A. Model of magnetic field

Based on the discussion of Sec. II, the following model assumptions are adopted:

- The 3-dimensional structure of solenoidal fields (magnetic field, vector potential, current density, solenoidal velocity) and scalar fields (ion and electron densities and temperatures, electric scalar potential) associated with the spontaneously self-organized state (SSS) in the DPF can be represented by a discrete spectrum consisting of low integer harmonics of eigenfunctions of the curl and of the associated Laplacian (with negative definite eigenvalues), respectively.
- The fundamental mode is assumed to be one that can be "fitted" to the umbrella shape of the sheath in some manner, not specified at this stage.
- This spectrum of eigenmodes stores the kinetic energy and momentum associated with the radial motion of the plasma after it is no longer able to continue the radial motion because of stagnation at the axis. The partitioning of this energy and momentum among various modes is left unspecified at this stage.

A background of turbulent fluctuations of electric and magnetic fields and plasma density over a wide spectrum of space and time scales also inevitably exists. The main discharge current that enters the plasma through the anode and leaves at the cathode and the associated azimuthal magnetic field are distinct from the closed current and magnetic field lines associated with the SSS. In terms of the RGV model,[57] the discharge current is related to the magnetic energy stored in the plasma inductance, while the closed loops of current and associated magnetic field are related to the work done in accelerating the plasma, which gets converted into energy of turbulent vortex cells at the moment of stagnation.

These model assumptions do not amount to a quantitative predictive model. Rather, they are deliberately intended to be broad enough to provide only a qualitative model of phenomenology associated with the acceleration and trapping of ions in bounded trajectories. This is in keeping with the current state of relevant experimental evidence in DPF physics, which consists of isolated reports, many of them published as conference papers or dissertations, from facilities that no longer exist, with no systematic follow-up investigations, which have been routinely ignored by the plasma focus community for decades.

In view of experimental observations of a fixed orientation of the axial magnetic field,[6] and absence of large scale *periodic* azimuthal structure of the observed spontaneous state,[32] it is appropriate to

assume that the observed state is *not* an equal mixture of curl eigenfunctions with both values of handedness index s and that the azimuthal mode number m is zero. The fundamental CK mode and its principal harmonics associated with the SSS are, therefore, assumed to be described by the expression

$$\vec{\chi}_{\kappa\gamma} \equiv \vec{\chi}_{poloidal} + \vec{\chi}_{toroidal},$$

$$\vec{\chi}_{poloidal} = k^{-2}\left(\kappa\gamma J_1(\gamma r)\sin(\kappa z)\hat{r} + \gamma^2 J_0(\gamma r)\cos(\kappa z)\hat{z}\right), \quad (15)$$

$$\vec{\chi}_{toroidal} = k^{-1}\gamma J_1(\gamma r)\cos(\kappa z)\hat{\theta},$$

where the radial mode number γ takes values $\gamma_p \equiv p\gamma_1$, the axial mode number takes values $\kappa_q \equiv \pm q\kappa_1$, and the eigenvalue k has values $k_{p,q} \equiv \sqrt{\gamma_p^2 + \kappa_q^2}$, where p and q are positive integers. The radial and axial mode numbers γ_1 and κ_1 of the fundamental mode are assumed to be related to the DPF anode radius a as $\gamma_1 = \tilde{\gamma}_1 a^{-1}$, $\kappa_1 = \tilde{\kappa}_1 a^{-1}$, where $\tilde{\gamma}_1$ and $\tilde{\kappa}_1$ are model constants and $\tilde{k}_{p,q} \equiv \sqrt{\tilde{\gamma}_p^2 + \tilde{\kappa}_q^2}$. The RGV model scales all lengths to the anode radius, effectively treating a as unity. Unless otherwise stated, lengths will be assumed to be scaled to a and radial and axial mode numbers scaled to a^{-1} and such scaled quantities shall be denoted with an overtilde.

A field line of $\vec{\chi}_{\kappa\gamma}$ passing through a given point (r_0, θ_0, z_0) is given by

$$\frac{dr}{\hat{r} \cdot \vec{\chi}_{\kappa\gamma}} = \frac{rd\theta}{\hat{\theta} \cdot \vec{\chi}_{\kappa\gamma}} = \frac{dz}{\hat{z} \cdot \vec{\chi}_{\kappa\gamma}} = \frac{ds}{|\vec{\chi}_{\kappa\gamma}(r_0, \theta_0, z_0)|}. \quad (16)$$

It can be shown that the surface $\Sigma(\tilde{r}, \tilde{z}) = \tilde{\gamma}\tilde{r}J_1(\tilde{\gamma}\tilde{r})\cos(\tilde{\kappa}\tilde{z})$ = constant has a gradient that is perpendicular to $\vec{\chi}_{\kappa\gamma}$ at every point so that the field line passing through a given point (r_0, θ_0, z_0) spans the surface $\Sigma(\tilde{r}, \tilde{z}) = \Sigma(\tilde{r}_0, \tilde{z}_0)$. In other words, Σ can be considered as a family of flux surfaces associated with the solenoidal field $\vec{\chi}_{\kappa\gamma}$. The associated Helmholtz mode is given by

$$\Psi = J_0(\tilde{\gamma}\tilde{r})\cos(\tilde{\kappa}\tilde{z}). \quad (17)$$

The relation of a field line of the fundamental CK mode with the umbrella shape of the DPF sheath in the present model is illustrated in Fig. 1.

A better appreciation of the spatial structure of the solenoidal field $\vec{\chi}_{\kappa\gamma}$ can be obtained by looking at the family of flux surfaces Σ (see Fig. 2). These are disjoint families of nested tori centered on the zeroes $j_{0,n}$ of $J_0(\tilde{\gamma}\tilde{r})$ and $\pm n'\pi$ of $\sin(\tilde{\kappa}\tilde{z})$, which may be labeled by the orders (n, n') of the zeroes.

The Helmholtz mode, which is the basis set for scalar fields such as density and temperature, has a central peak located on the axis and is seen to mimic the plasmoid observed in PF-1000.[27,28] Since electron thermal conduction and diffusion is inhibited across, but not along, the magnetic field, it is reasonable to assume[32] that surfaces of constant temperature and density would be similar to flux surface Σ of the CK mode over time scale comparable with electron transit time but would resemble the Helmholtz mode over time scale comparable with Alfvén transit time. This mimics the PF-1000 observation that the SSS evolution begins with toroidal topology similar to Σ and then evolves into a plasmoidal topology similar to the Helmholtz mode. Note that both the CK
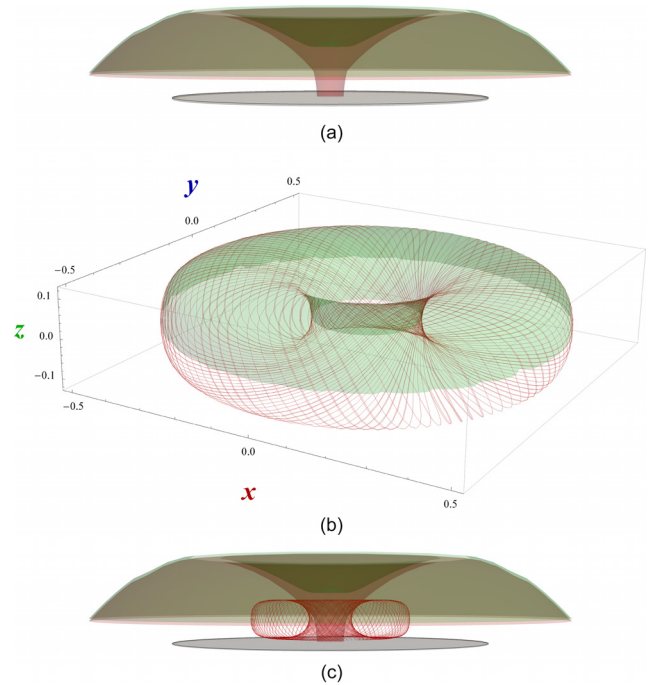

FIG. 1. (a) Umbrella-like shape characteristic of the DPF simulated using the RGV model. The dimensions are normalized to the anode radius. The anode is shown at the base of the umbrella shape. (b) A finite length of a *single field line* of the fundamental CK mode calculated from (16) with $\tilde{\gamma}_1 = 7$, $\tilde{\kappa}_1 = 10$, passing through the point $\tilde{r}_0 = 1/\tilde{\gamma}$, $\theta_0 = 0$, $\tilde{z}_0 = 0.4/\tilde{\kappa}$ superimposed on half the flux surface. The field $\vec{\chi}_{\kappa\gamma}$ is described by an infinity of such lines passing through an infinity of distinct points. (c) The field line superimposed over the umbrella profile of DPF to illustrate the relation between the proposed fundamental mode and plasma shape. Note that the anode center is at $\tilde{z} = -0.15$. The values of model constants $\tilde{\gamma}_1$ and $\tilde{\kappa}_1$ are chosen for clarity of illustration rather than any physical reasoning.

mode surface Σ and the Helmholtz mode surface Ψ have toroidal topology at $\tilde{z} = \pm\pi/\tilde{\kappa}$. Only positive contour values of Σ have an intuitive physical meaning and are displayed. This is the reason for the matrix-like appearance of the contour plot; the gaps are locations of negative-value contours of Σ. The radial boundaries of each set of nested tori of Σ are determined by the zeroes of $J_1(\tilde{\gamma}\tilde{r})$ while the axial boundaries are determined by zeros of $\cos(\tilde{\kappa}\tilde{z})$. The harmonics of the fundamental CK mode (p,q) have maxima at $\tilde{r}_{p,q,n} = j_{0,n}/p\tilde{\gamma}_1$; $\tilde{z}_{p,q,n'} = \pm n'\pi/q\tilde{\kappa}_1$, where $j_{0,n}$ is the nth zero of Bessel function $J_0(x)$. Figure 2(b) illustrates the array of toroids superimposed on the plasma profile.

It is clear that only those toroids which overlap with the plasma profile can possibly have a physical role in DPF dynamics. This implies that only the set of toroids closest to the axis need be taken into account in any theoretical consideration. Also, higher harmonics would occupy a proportionately much smaller volume and would therefore contain a smaller fraction of total energy and particle content. Hence, only the low harmonics need be considered. Figure 1(b) shows a plasmoid in the plasma stem and a toroid in the umbrella region for mode (3,3), similar to observations on PF-1000.[34] The evidence for existence of a current return path just outside the pinch enclosing a low density plasma bubble[20,35,36] is consistent with the structure of the CK modes and Helmholtz modes depicted in Fig. 2. It is not difficult to see that
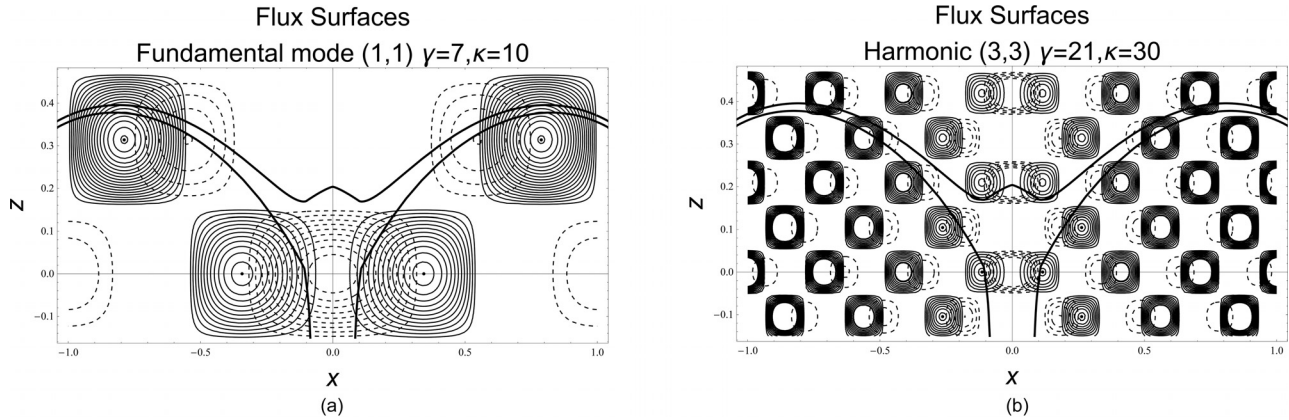
FIG. 2. (a) Contour plot of the flux surface $\Sigma(\tilde{r}, \tilde{z}) = \tilde{\gamma}\tilde{r}J_1(\tilde{\gamma}\tilde{r})\cos(\tilde{\kappa}\tilde{z})$ in Cartesian coordinates in the $y = 0$ plane for the fundamental mode (1,1) of Fig. 1, with $\tilde{\gamma}_1 = 7$ and $\tilde{\kappa}_1 = 10$. Local maxima of Σ occur at zeroes of $J_0\left(\tilde{\gamma}\sqrt{\tilde{x}^2 + \tilde{y}^2}\right)$ and $\sin(\tilde{\kappa}\tilde{z})$ while radial and axial boundaries occur at zeros of $J_1\left(\tilde{\gamma}\sqrt{\tilde{x}^2 + \tilde{y}^2}\right)$ and $\cos(\tilde{\kappa}\tilde{z})$. The dashed lines are contours of the $m = 0$ Helmholtz mode $\Psi = J_0(\tilde{\gamma}\tilde{r})\cos(\tilde{\kappa}\tilde{z})$. The dots marking centers of the nested toroids correspond to $(\pm j_{01}/\tilde{\gamma}, 0)$ and $(\pm j_{0,2}/\tilde{\gamma}, \pm\pi/\tilde{\kappa})$ where $j_{0,1} = 2.4048$, $j_{0,2} = 5.52008$. Only positive contour values are displayed. (b) The Harmonic mode (3,3). Note the (Helmholtz mode) plasmoid in the plasma stem and the toroid in the umbrella shape (shown by dashed lines). Harmonics are simply scaled versions of the fundamental mode.

for some harmonic, a "ball-like structure" could appear in the interferogram near the edge of the plasma stem, as observed in PF-1000[58] and a larger number of plasmoids could appear in the stem or indeed in the apparently empty regions outside the dense plasma stem, which could be the source of discrete ion sources observed in Ref. 36. These observations confirm that the present model is in qualitative agreement with observed PF-1000 phenomenology.

One can express the magnetic field, current density, vector potential, and solenoidal part of electric field associated with the SSS as

$$
\begin{aligned}
\vec{B}_{SSS} &= \sum_{p,q} B_0^{(p,q)} T^{(p,q)}(t)\vec{\chi}_{\kappa_p\gamma_q}, \\
\vec{A}_{SSS} &= \sum_{p,q} B_0^{(p,q)} T^{(p,q)}(t)k_{p,q}^{-1}\vec{\chi}_{\kappa_p\gamma_q}, \\
\vec{J}_{SSS} &= \mu_0^{-1} \sum_{\pm p,q} B_0^{(p,q)} T^{(p,q)}(t)k_{p,q}\vec{\chi}_{\kappa_p\gamma_q}, \\
\vec{E}_{SSS} &= -\sum_{p,q} B_0^{(p,q)}\dot{T}^{(p,q)}(t)k_{p,q}^{-1}\vec{\chi}_{\kappa_p\gamma_q},
\end{aligned}
\tag{18}
$$

where $T^{(p,q)}(t)$ is the temporal profile of the (p,q) mode and $B_0^{(p,q)}$ is its amplitude. The current flowing in the z-direction in the (p,q) mode (poloidal current $I_{pol}^{(p,q)}$) can be found by integrating the z-component of current density at its mid-plane from its inner boundary at zero radius to its first zero at $j_{0,1}/\tilde{\gamma}_1$

$$
I_{pol}^{(p,q)} = \mu_0^{-1}B_0^{(p,q)}2\pi\tilde{k}_{p,q}^{-1}a(j_{0,1})J_1(j_{0,1}).
\tag{19}
$$

This yields

$$
B_0^{(p,q)} = \frac{\mu_0 I_{pol}^{(p,q)}\tilde{k}_{p,q}}{2\pi a(j_{0,1})J_1(j_{0,1})}.
\tag{20}
$$

B. Ion trajectories in model magnetic field

In order to examine the question of ion trapping,[22,23] the nature of ion orbits in this 3-dimensional magnetic field needs to be

appreciated. Let $\vec{R}_i(t)$ be the instantaneous position vector of an ion. The ion trajectories are then given by the equation

$$
\begin{aligned}
\frac{d\vec{R}_i}{dt} &= \vec{v}_i \\
\frac{d\vec{v}_i}{dt} &= \frac{e}{m_i}\left(\vec{E}(\vec{R}_i, t) + \vec{v}_i \times \vec{B}(\vec{R}_i, t)\right),
\end{aligned}
\tag{21}
$$

where $\vec{E}(\vec{R}_i, t)$ $\vec{B}(\vec{R}_i, t)$ are the local instantaneous electric and magnetic fields at the instantaneous position of the ion. Since the flux surfaces of the fundamental mode and its harmonics form nested regions, it is reasonable to first study ion trajectories associated with each of the regions separately and then consider the combined effect of multiple modes. The following discussion aims to classify ion trajectories according to their properties.

1. Ion trajectories in single stationary CK mode

As a first step, the properties of ion trajectories in stationary magnetic field corresponding to a single CK mode are considered.

Rewriting (21) in non-dimensionalized coordinates $\underline{R}_i \equiv a^{-1}\vec{R}_i \equiv \tilde{r}_i\hat{r} + \tilde{r}_i\theta_i\hat{\theta} + \tilde{z}_i\hat{z}$ and time $\tau \equiv eB_0^{(p,q)}t/2\pi m_i$,

$$
\begin{aligned}
\frac{d\underline{R}_i}{d\tau} &= \frac{2\pi m_i}{eB_0^{(p,q)}a}\vec{v}_i \equiv \underline{v}_i, \\
\frac{d\underline{v}_i}{d\tau} &= 2\pi\left(-\dot{T}^{(p,q)}(\tau)\left(\tilde{k}_{p,q}\right)^{-1}\vec{\chi}_{\kappa_p\gamma_q}(\underline{R}_i, \tau)\right. \\
&\quad \left. +T^{(p,q)}(\tau)\underline{v}_i \times \vec{\chi}_{\kappa_p\gamma_q}(\underline{R}_i, \tau)\right).
\end{aligned}
\tag{22}
$$

Note that the ion kinetic energy is normalized to the quantity

$$
\mathcal{E}_0^{(p,q)}(eV) = \frac{1}{2}\frac{m_i}{e}\left(\frac{eB_0^{(p,q)}a}{2\pi m_i}\right)^2 \approx 6.23 \times 10^4\tilde{k}_{p,q}^2\left(I_{pol}^{(p,q)}(MA)\right)^2,
\tag{23}
$$

and the time is measured in units of Larmor periods corresponding to the peak amplitude of the CK mode being considered.

Explicitly writing the second of equations (22) in cylindrical coordinates, one gets

$$\frac{d^2\tilde{r}_i}{d\tau^2} - \tilde{r}_i\left(\frac{d\theta}{d\tau}\right)^2 = -2\pi\dot{T}^{(p,q)}(\tau)\left(\tilde{k}_{p,q}\right)^{-1}\left(\tilde{\gamma}_p/\tilde{k}_{p,q}\right)$$
$$\times\left(\tilde{\kappa}_q/\tilde{k}_{p,q}\right)J_1(\gamma_p r)\sin(\tilde{\kappa}\tilde{z})$$
$$+2\pi T^{(p,q)}(\tau)\left(\tilde{r}_i\frac{d\theta_i}{d\tau}\left(\tilde{\gamma}_p/\tilde{k}_{p,q}\right)^2 J_0(\tilde{\gamma}_p\tilde{r}_i)\cos(\tilde{\kappa}_q\tilde{z}_i)\right.$$
$$\left.-\frac{d\tilde{z}_i}{d\tau}\left(\tilde{\gamma}_p/\tilde{k}_{p,q}\right)J_1(\tilde{\gamma}_p\tilde{r}_i)\cos(\tilde{\kappa}_q\tilde{z}_i)\right), \quad (24)$$

$$\tilde{r}_i\frac{d^2\theta_i}{d\tau^2} + 2\frac{d\tilde{r}_i}{d\tau}\frac{d\theta_i}{d\tau} = -2\pi\dot{T}^{(p,q)}(\tau)\left(\tilde{k}_{p,q}\right)^{-1}\left(\tilde{\gamma}_p/\tilde{k}_{p,q}\right)J_1(\tilde{\gamma}_p\tilde{r})\cos(\tilde{\kappa}_q\tilde{z})$$
$$+2\pi T^{(p,q)}(\tau)\left(\frac{d\tilde{z}_i}{d\tau}\left(\tilde{\gamma}_p/\tilde{k}_{p,q}\right)\left(\tilde{\kappa}_q/\tilde{k}_{p,q}\right)J_1(\tilde{\gamma}_p\tilde{r}_i)\right.$$
$$\left.\times\sin(\tilde{\kappa}_q\tilde{z}_i) - \frac{d\tilde{r}_i}{d\tau}\left(\tilde{\gamma}_p/\tilde{k}_{p,q}\right)^2 J_0(\tilde{\gamma}_p\tilde{r}_i)\cos(\tilde{\kappa}_q\tilde{z}_i)\right),$$

$$\frac{d^2\tilde{z}_i}{d\tau^2} = -2\pi\dot{T}^{(p,q)}(\tau)\left(\tilde{k}_{p,q}\right)^{-1}\left(\tilde{\gamma}_p/\tilde{k}_{p,q}\right)^2 J_0(\gamma_p r_i)\cos(\tilde{\kappa}_q\tilde{z}_i) \quad (25)$$
$$+2\pi T^{(p,q)}(\tau)\left(\frac{d\tilde{r}_i}{d\tau}\left(\tilde{\gamma}_p/\tilde{k}_{p,q}\right)J_1(\tilde{\gamma}_p\tilde{r}_i)\cos(\tilde{\kappa}_q\tilde{z}_i)\right.$$
$$\left.-\tilde{r}_i\frac{d\theta_i}{d\tau}\left(\tilde{\gamma}_p/\tilde{k}_{p,q}\right)\left(\tilde{\kappa}_q/\tilde{k}_{p,q}\right)J_1(\tilde{\gamma}_p\tilde{r}_i)\sin(\tilde{\kappa}_q\tilde{z}_i)\right). \quad (26)$$

The initial conditions are left unspecified; they form part of a specific initial value problem being studied. The ion acceleration problem in plasma focus would in principle be a collection of a large number of such initial value problems, which could, however, be qualitatively grouped into a smaller number of categories.

The following expressions can be verified using (24)–(26):

$$\frac{d}{d\tau}\left(\tilde{r}_i^2\frac{d\theta_i}{d\tau} + 2\pi\tilde{k}_{p,q}^{-1}T^{(p,q)}(\tau)\vec{\chi}_{\kappa_p\gamma_q}(\tilde{r}_i,\tilde{z}_i)\cdot\hat{\theta}\right)$$
$$= 2\pi\tilde{k}_{p,q}^{-1}\dot{T}^{(p,q)}(\tau)\vec{\chi}_{\kappa_p\gamma_q}(\tilde{r}_i,\tilde{z}_i)\cdot\hat{\theta}, \quad (27)$$

$$\frac{d}{d\tau}\left(\left(\frac{d\tilde{r}_i}{d\tau}\right)^2 + \tilde{r}_i^2\left(\frac{d\theta_i}{d\tau}\right)^2 + \left(\frac{d\tilde{z}_i}{d\tau}\right)^2\right)$$
$$= -4\pi\left(\tilde{k}_{p,q}\right)^{-1}\dot{T}^{(p,q)}(\tau)\vec{\chi}_{\kappa_p\gamma_q}(\tilde{r}_i,\tilde{z}_i)\cdot\underline{v}_i. \quad (28)$$

For the case of stationary magnetic fields, $\dot{T}^{(p,q)}(\tau) = 0$, these relations correspond to the well-known results on conservation of canonical angular momentum and ion kinetic energy in axisymmetric stationary magnetic fields in the dimensionless notation adopted above. The ion trajectories can, therefore, be labeled by the non-dimensional quantities λ and ϵ proportional to conserved angular momentum and kinetic energy, respectively,

$$\lambda \equiv \tilde{r}_i^2\frac{d\theta_i}{d\tau} + \frac{2\pi}{\tilde{k}_{p,q}^2}\tilde{\gamma}_p\tilde{r}_iJ_1(\tilde{\gamma}_p\tilde{r}_i)\cos(\tilde{\kappa}_q\tilde{z}_i), \quad (29)$$

$$\epsilon \equiv \left(\frac{d\tilde{r}_i}{d\tau}\right)^2 + \tilde{r}_i^2\left(\frac{d\theta_i}{d\tau}\right)^2 + \left(\frac{d\tilde{z}_i}{d\tau}\right)^2. \quad (30)$$

Equation (30) is equivalent to a two dimensional potential well problem

$$\epsilon_P \equiv \left(\frac{d\tilde{r}_i}{d\tau}\right)^2 + \left(\frac{d\tilde{z}_i}{d\tau}\right)^2$$
$$= \epsilon - \tilde{r}_i^{-2}\left(\lambda - 2\pi\tilde{k}_{p,q}^{-2}\tilde{\gamma}_p\tilde{r}_iJ_1(\tilde{\gamma}_p\tilde{r}_i)\cos(\tilde{\kappa}_q\tilde{z}_i)\right)^2. \quad (31)$$

The Left Hand Side (LHS) of (31) is proportional to the kinetic energy associated with poloidal component of ion trajectory; it would, therefore, be appropriate to refer to the Right Hand Side of (31) as a poloidal potential well (PPW). The ion trajectories are localized within a region defined by

$$V_{\epsilon,\lambda}(\tilde{r},\tilde{z}) \equiv \epsilon - \tilde{r}_i^{-2}\left(\lambda - 2\pi\tilde{k}_{p,q}^{-2}\tilde{\gamma}_p\tilde{r}_iJ_1(\tilde{\gamma}_p\tilde{r}_i)\cos(\tilde{\kappa}_q\tilde{z}_i)\right)^2 \geq 0. \quad (32)$$

Figure 3 shows the contour plots of the function $V_{\epsilon,\lambda}(\tilde{r},\tilde{z})$ in Cartesian coordinates for various values of ϵ and λ.

Figure 3(a) shows the case of zero canonical angular momentum. The contours are closed curves representing nested toroidal surfaces, localized within the CK modes shown in Fig. 2. The innermost curve corresponds to $V_{\epsilon,0}(\tilde{r},\tilde{z}) = 0$ for which ion motion in the $(\tilde{r},\tilde{z})$ plane is absent—the trajectories are simply circular orbits that maintain a constant radial coordinate $\tilde{r}_0$ and remain at a constant elevation $\tilde{z}_0$. There are no open contours suggesting that *ions never escape these trajectories.*

Figure 3(b) illustrates a case of small positive canonical angular momentum. The contours localized within the central CK mode remain closed curves but those away from the mid plane have both closed curves and open curves. The open curves resemble a beam emitted along the axis.

Figure 3(c) illustrates a case of small negative canonical angular momentum. The contours localized within the central CK mode now have a mixture of closed curves, indicating trajectories that remain within the mode and open curves which resemble a beam along the axis.

Some estimates of typical ion energy may be obtained as follows. For circular orbits with $\epsilon_P = 0$, the parameter ϵ can be expressed as a function of λ, $\tilde{r}_0$, and $\tilde{z}_0$

$$\epsilon_{circ} = \tilde{\gamma}_p^2\left(\tilde{\gamma}_p\tilde{r}_0\right)^{-2}\left(\lambda - 2\pi\tilde{k}_{p,q}^{-2}\tilde{\gamma}_p\tilde{r}_0J_1(\tilde{\gamma}_p\tilde{r}_0)\cos(\tilde{\kappa}_q\tilde{z}_0)\right)^2. \quad (33)$$

The expression $\tilde{\gamma}_p\tilde{r}_0J_1(\tilde{\gamma}_p\tilde{r}_0)\cos(\tilde{\kappa}_q\tilde{z}_0)$ equals zero at $\tilde{\gamma}_p\tilde{r}_0 = 3.83171$ and/or $\tilde{\kappa}_q\tilde{z}_0 = \pm\pi/2$ and has a maximum value of 1.24846 at $\tilde{\gamma}_p\tilde{r}_0 = 2.40483$ and $\tilde{\kappa}_q\tilde{z}_0 = 0$. The parameter ϵ_{circ} therefore must lie between the limits $\epsilon_1 = 0.068\tilde{\gamma}_p^2\lambda^2$ (for circular orbits near the boundaries of the stationary CK mode, see Fig. 2) and $\epsilon_2 = 0.173\tilde{\gamma}_p^2(\lambda - 7.844\tilde{k}_{p,q}^{-2})^2$ (for circular orbits near the center of the stationary CK mode). It is seen that

$$\frac{\epsilon_2}{\epsilon_1} - 1 = \frac{1.544\left(\lambda - 4.83\tilde{k}_{p,q}^{-2}\right)\left(\lambda - 21.03\tilde{k}_{p,q}^{-2}\right)}{\lambda^2}. \quad (34)$$
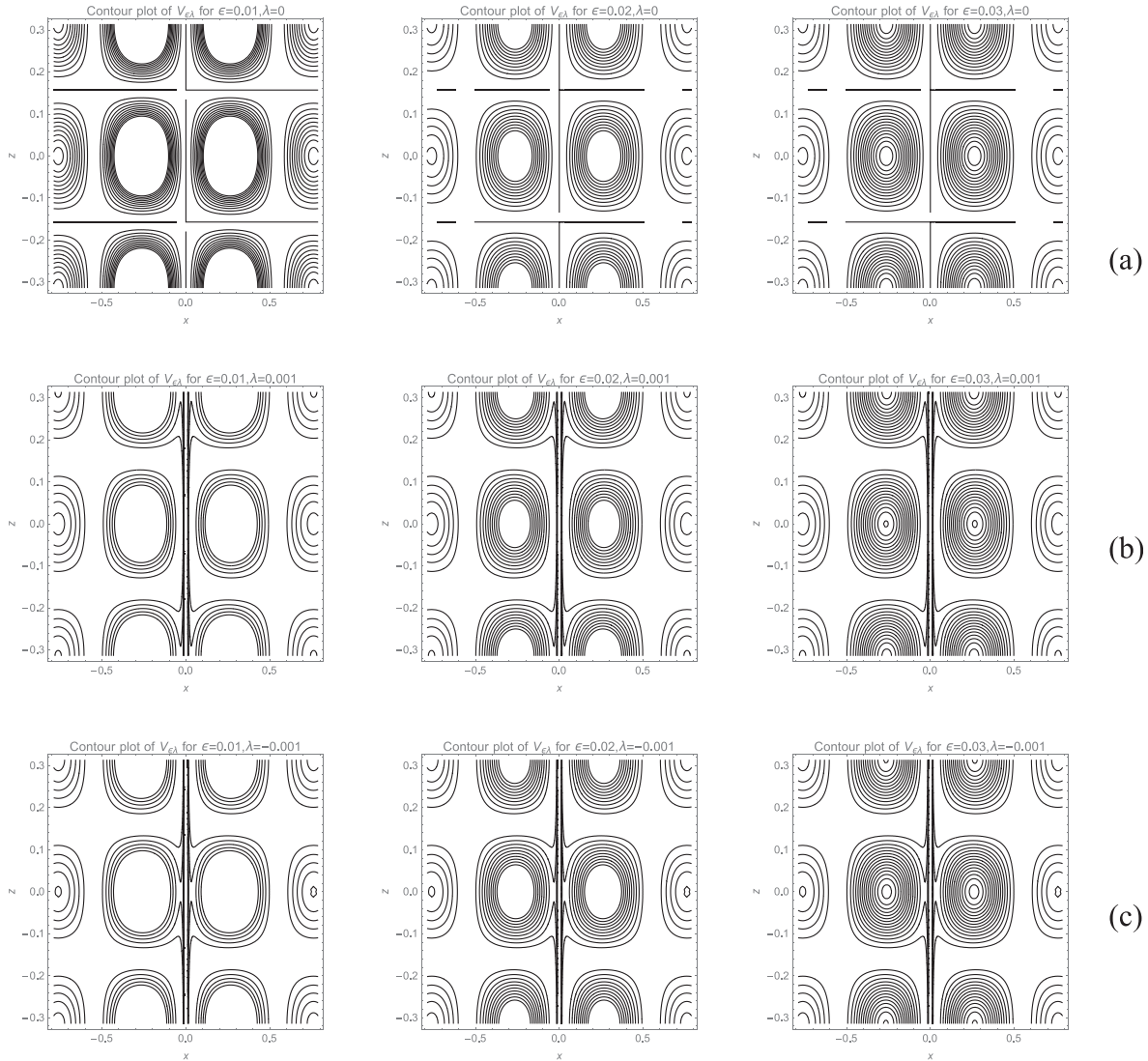
FIG. 3. Contour plots of the function $V_{\epsilon,\lambda}(\tilde{r},\tilde{z})$ with λ taking values 0, 0.001, -0.001, and ϵ taking values 0.01, 0.02, and 0.03, with $\tilde{\gamma}_1 = 7$ and $\tilde{\kappa}_1 = 10$ as for Figs. 1 and 2. The plot shows positive-valued contours spaced by 0.002 starting with the innermost contour at zero.

For $\lambda < 4.83\tilde{k}_{p,q}^{-2}$ or $\lambda > 21.03\tilde{k}_{p,q}^{-2}$, the circular orbits near the center have more energy than those near the mode boundaries. For $4.83\tilde{k}_{p,q}^{-2} < \lambda < 21.03\tilde{k}_{p,q}^{-2}$, the circular orbits near the mode boundaries have more energy than those near the mode center. For the special case of $\lambda = 0$, the circular orbits have a maximum energy $\epsilon_{2max} = 10.64\tilde{\gamma}_p^2\tilde{k}_{p,q}^{-4}$ near the mode center. For the parameters of Fig. 3, $\epsilon_{2max} \approx 0.023483$.

These estimates give a rough idea about the energy range of ions that are likely to populate the circular orbits. The ensemble of circular orbits of all possible energies can be visualized as a collection of the innermost contours for ϵ varying between the limits mentioned above.

For nonzero values of $\eta \equiv \epsilon_P/\epsilon$, there would be a poloidal component of ion trajectory. If the poloidal velocity is nonzero at the edge

of the CK mode (zeroes of $J_1(\tilde{\gamma}_p\tilde{r}_i)\cos(\tilde{\kappa}_q\tilde{z}_i)$), the ion escapes the CK mode. From (31), an approximate criterion for ion escape from CK mode can be written as

$$\eta > \eta_m \equiv 1 - \left(\frac{\tilde{\gamma}_p}{j_{1,n}}\right)^2\frac{\lambda^2}{\epsilon}. \tag{35}$$

Ions below this limit are likely to have trajectories which can be described as having toroidal directionality.

The point of this discussion is the observation that purely circular orbits have a very large path length (theoretically infinite) compared with the radial and axial dimensions of the CK mode. The trajectories that have a limited amount of poloidal motion as defined by (35) should still have path length larger than the mode dimensions. Those

that have larger amount of motion in the $(\tilde{r}, \tilde{z})$ plane have path lengths on the order of the mode dimensions. Neutrons that result from interaction between the accelerated deuterons in circular orbits and the background warm plasma are, therefore, likely to be more abundant than neutrons from any other kind of ion trajectories. They would have center-of-mass (CM) velocity directed perpendicular to the axis and have laterally mirror-symmetric Doppler-shifted spectra in agreement with observations.[16,18,19] Neutrons that result from deuterons in trajectories with significant but limited poloidal motion that keeps them confined to the poloidal potential well would exhibit shift of neutron spectra to higher energy in both positive and negative axial directions (but at spatially separated positions) and signature of a looping motion in $(\tilde{r}, \tilde{z})$ plane as experimentally observed.[8–11,13–15,18] Both sets of neutrons would be emitted over a time much larger than the deuteron transit time across the plasma dimensions.[17] The circular orbits would contribute a significant neutron yield even if the CK mode has only partial overlap with the dense plasma because of the larger number of passes through the less dense medium surrounding the dense plasma. This would account for the fact that the size of the reaction zone seen in time integrated ion pinhole pictures is larger than the size of the dense plasma.[16,20,34]

The ions which escape the CK mode because of their poloidal energy being larger than the limit (35) would be detected by ion pinhole cameras. The observation of sources of accelerated deuterons coming from a region external to the dense plasma[36] is in agreement with the proposed model of the magnetic field and of the ion trajectories in single CK modes discussed above. The shape of open curves in the contour map of Fig. 3 is strongly suggestive of low divergence ion beams emitted along the axis, which have been observed since early days of plasma focus research.[59]

2. Ion trajectories in single quasi-stationary CK mode

In reality, the single CK mode will not be stationary. It must begin at some time and end after some time. The case when time scale of this evolution is much longer than the instantaneous Larmor period can be termed "quasi-stationary" (QS). The quantities λ and ϵ discussed above are then no more "constants" of motion and are expected to slowly change with time. This is a problem with two time scales and the interest is in the scenario at the longer time scale. The quantity $\dot{T}(\tau)/T(\tau)$ is then a small parameter $\sim \alpha \ll 1$. One may still define parameters $\lambda(\alpha^{-1}\tau)$ proportional to canonical angular momentum and $\epsilon(\alpha^{-1}\tau)$ proportional to ion kinetic energy which slowly vary with time using (27) and (28)

$$\lambda(\alpha^{-1}\tau) \equiv \tilde{r}_i^2 \frac{d\theta_i}{d\tau} + 2\pi \tilde{k}_{p,q}^{-1} T^{(p,q)}(\alpha^{-1}\tau) \vec{\chi}_{\kappa_p \gamma_q} \cdot \hat{\theta}, \qquad (36)$$

$$\epsilon(\alpha^{-1}\tau) \equiv \left(\frac{d\tilde{r}_i}{d\tau}\right)^2 + \tilde{r}_i^2 \left(\frac{d\theta_i}{d\tau}\right)^2 + \left(\frac{d\tilde{z}_i}{d\tau}\right)^2. \qquad (37)$$

Discussion of Subsection III B 1 involving the existence of poloidal potential well might then be applicable to this case leading to the following qualitative results:

1. There exist circular orbits having negligible motion in the $(\tilde{r}, \tilde{z})$ plane, which pass repeatedly through a toroidal region centered around $(\tilde{r}_0, \tilde{z}_0)$ described by the relation

$$\epsilon(\alpha^{-1}\tau) = \tilde{r}_0^{-2}(\lambda(\alpha^{-1}\tau) - 2\pi \tilde{k}_{p,q}^{-2} T^{(p,q)}(\alpha^{-1}\tau) \tilde{\gamma}_p \tilde{r}_0 J_1(\tilde{\gamma}_p \tilde{r}_0) \cos(\tilde{\kappa}_q \tilde{z}_0))^2 \qquad (38)$$

2. It evolves over a longer time than the ion Larmor period. The circular orbits would have a much smaller path length as compared to the stationary case that would depend on the duration of the mode but it still is expected to be larger than the mode dimensions.

3. For ion trajectories that have a significant motion in the $(\tilde{r}, \tilde{z})$ plane, there exists a threshold poloidal kinetic energy above which the ions escape the CK mode.

4. The expected nature of neutron emission discussed earlier for the case of stationary CK mode should therefore be valid qualitatively for the quasi-stationary case except that the validity should last over a smaller time period.

3. Ion trajectories in single non-stationary (transient) CK mode

When the CK mode grows and decays on time scales comparable with the instantaneous Larmor period, there are no constants of motion and the ion trajectories are not confined to a region definable in terms of invariants. This mode would be truly non-stationary or transient mode (T-mode). The associated induced electric field is expected to accelerate ions with trajectories that strongly depend on the initial position of the ion, the mode structure, and its time profile. These would interact with the background plasma for a duration not much larger than transit time of an ion across plasma dimensions. Therefore, their contribution to the neutron emission would be low but their presence will be more strongly represented in ion pinhole pictures than that of the ion trajectories that are confined in the quasi-stationary poloidal potential well.

4. Ion trajectories in a superimposition of CK modes

The model magnetic field described above is a mixture of several CK modes, each with its own time history of growth, persistence, and decay and each of which may be classified as quasi-stationary or non-stationary at different times depending on the mode amplitude. The discussion of Sec. II suggests that the lower end of mode number spectrum (larger physical size of the mode) would be more likely to fall into a QS category. Higher harmonics and modes at the high mode number end of the spectrum are likely fall into the transient category. The T-modes could accelerate ions that escape but which could remain trapped in the poloidal potential well of a larger QS mode that surrounds the T-mode. If the T-mode coincides with the rise of the QS mode, the acceleration of the ions injected by the T-mode would start at an already high initial velocity. Depending on its energy and angular momentum, it could populate circular or toroidal trajectories of the poloidal potential well associated with the QS mode contributing significantly to the neutron emission or escape and be detected by ion diagnostics.

C. Summary of the above discussion

The main issues revealed by the experimental evidence revisited in Introduction can be summarized as follows:

1. Growth, persistence, and decay of bounded magneto-plasma structures beginning slightly before the stagnation of the plasma at the axis appears to be a well-established phenomenon with 15 frame interferometry and magnetic probes as principal diagnostics.

2. The early phase of neutron emission starts well before the plasma stagnation/current derivative singularity and reaches a first maximum well before the instability.

3. Properties such as fluence and spectral anisotropy, energy spectra (with or without time or space resolution) and time duration of the neutron emission in comparison with the transit time of deuterons that cause neutrons are consistent with confinement of $\sim$100 keV deuterons for tens of transit times across the plasma diameter. The CM motion of these deuterons has features of motion in the azimuthal direction as well as poloidal direction.

4. If the acceleration of ions involves an electric field, its effect on electrons should involve creation of energetic electrons and hard x-rays (HXRs) which should have an observable correlation with neutron emission. Information about such correlation or its absence is very scarce.

5. The experimental evidence offers no clue to pinpoint which aspects of plasma dynamics hold the key to explaining these features.

In this context, the qualitative model discussed above offers the following narrative:

a) Nonlinear plasma dynamics expressed in cylindrical Fourier space using eigenfunctions of curl as complete orthonormal basis (COB) for solenoidal fields, eigenfunctions of Laplacian as COB for scalar fields, gradient of the latter as COB for irrotational fields leads to evolution equations in cylindrical mode number space. The Spectral Amplitude Density (SAD) of each field tends to concentrate toward lower and high ends of mode number spectrum subject to physical constraints because nonlinear terms in plasma dynamics generate evolution at sum and difference of mode numbers of interacting modes. Evolution dynamics puts a lower limit to radial and axial mode numbers in terms of the finite size of the plasma and makes the lowest azimuthal mode number zero in accordance with the carefully engineered azimuthal symmetry of the plasma. This process leads to growth, persistence and decay of large scale magneto-plasma structures that can be visualized using interferometry, Schlieren or soft x-ray pinhole camera. Conservation of energy and momentum associated with the radial motion of the plasma that is interrupted when the plasma reaches the axis probably plays a role in this process. This narrative is in agreement with all the qualitative features of phenomenology of SSS reported so far as discussed in detail above.

b) Ion motion in a stationary *symmetric* curl eigenfunction state is equivalent to motion in a two dimensional poloidal potential well that is characterized by two constants of motion. This motion can be a purely circular orbit or a circular orbit superimposed with a small poloidal component of motion (toroidal trajectory) or a trajectory that escapes the curl eigenfunction state. The three kinds of trajectories have different residence time within the curl eigenfunction state.

c) The evolution of the mode spectrum might lead to a temporary condition where some modes can approximate a stationary, symmetric state for a limited time, where the ion motion may be simulated by a poloidal potential well characterized by two approximate "constants of motion" which vary on a time scale slower than the ion transit time across the well. This leads to increased residence time of ions within spatial boundaries of specific curl eigenfunction states for ions with circular and toroidal trajectories, leading to increased duration of neutron emission, features of rotational and poloidal motion in the CM motion inferred from neutron spectroscopy. This is in agreement with all qualitative features of neutron emission reported so far as discussed in detail above.

d) The proposed narrative concerning acceleration and trapping of ions involves their mass, and it clearly is not applicable for electrons in any direct manner.

e) This narrative suggests that the main aspects of plasma dynamics that are responsible for the observed qualitative properties of neutron emission are as follows: (a) symmetry of the plasma as it reaches the axis, (b) the fraction of total energy that is coupled to the radial motion which needs to be transferred to the turbulent cascade, and (c) existence of a preferred orientation of the poloidal magnetic field.

This is a *plausible narrative* consistent with all the observations mentioned in the Introduction and with basic physical principles. Its main problem is the absence of direct confirmation by targeted diagnostic measurements. Section IV identifies some diagnostic schemes which are feasible, untried, and focused on direct observation of unique features of this narrative. Once relevant quantitative data becomes available, the narrative can be further refined in terms of a *quantitative* model.

IV. DIAGNOSTICS POSSIBILITIES

The key signatures of the above narrative are as follows:

1. Emergence, persistence, and decay of a 3-dimensional *symmetric* magnetic field structure correlated in time with plasma stagnation/current derivative singularity. The poloidal component of this magnetic field structure requires the existence of an azimuthal (toroidal) current density distribution with a finite axial extent.

2. Lateral asymmetry in space-resolved neutron energy spectrum observed perpendicular to the axis expected from circular motion of deuterons

3. Complementary radial variation of space-resolved neutron energy spectrum observed at 0° and 180° to the axis expected from toroidal motion of ions trapped in a poloidal potential well.

4. Space and time correlation between the reaction zone and the symmetric magnetic structure.

5. Possible differences in the spatio-temporal distribution of hard x-rays and neutrons because of the mass-dependence of the constants of motion in the proposed narrative.

This section looks at some diagnostic schemes, which are feasible, untried, and sensitive to the above signatures of the proposed narrative. The last aspect (sensitivity) implies that failure to observe the expected signal in a well-designed experiment would be a strong,

unambiguous proof that the expected feature is absent leading to refutation of the proposed model.

A. Emergence, persistence, and decay of symmetric magnetic field structure

The generalized Ohm's law gives an expression for the electric field as

$$\vec{E} = -\vec{v} \times \vec{B} + \eta\vec{J} + (en)^{-1}\left(\vec{J} \times B - \vec{\nabla}p_e\right). \qquad (39)$$

At any time, the plasma has a charge density given by

$$\rho = \varepsilon_0\vec{\nabla} \cdot \vec{E}. \qquad (40)$$

The radial velocity of the plasma and the azimuthal magnetic field together create an axial component of the electric field that acquires an axial variation as the umbrella-shaped plasma approaches the axis and starts getting reflected. Thus, *the onset of plasma stagnation should be* accompanied by *a spike in the electric charge density on the plasma.*

The symmetric CK mode has an azimuthal current density associated with it [see (18)]

$$J_\theta = \mu_0^{-1}B_0^{(p,q)}T^{(p,q)}(t)\gamma_p J_1(\gamma_p r)\cos(\kappa_q z). \qquad (41)$$

Now, consider an open-ring-shaped conductor, having inner radius R, outer radius $R + \Delta R$, $\Delta R \ll R$, thickness d, and angular span $0°$ to $2\pi - \delta$, $\delta \ll 2\pi$ situated symmetrically about the device axis, *outside the cathode* and at an elevation z_0 close to the anode surface in a coordinate system in which $z = 0$ is the mid plane of the CK mode. Using standard results of electromagnetic theory, the scalar and vector potentials at any point on the conductor can be written as

$$\phi(\vec{r}, t) = \frac{1}{4\pi\varepsilon_0}\int d^3\vec{r}' \frac{\rho(\vec{r}', t')}{|\vec{r} - \vec{r}'|}; \quad t' = t - |\vec{r} - \vec{r}'|/c, \qquad (42)$$

$$A_\theta(\vec{r}) = \frac{\mu_0}{4\pi}\int d^3\vec{r}' \frac{J_\theta(\vec{r}', t')}{|\vec{r} - \vec{r}'|}. \qquad (43)$$

For plasma focus dimensions and timescales, $|\vec{r} - \vec{r}'|/c$ can be neglected. In the absence of an azimuthal electric field, the conducting ring would be an equipotential surface having scalar potential equal to the volume average of (42)

$$\phi_{ring}(t) = \frac{1}{2\pi}\int_0^{2\pi-\delta} d\theta\phi(R, \theta, z_0, t). \qquad (44)$$

However, the azimuthal electric field

$$E_\theta(\vec{r}, t) = -\partial_\theta\phi(\vec{r}, t) - \partial_t A_\theta \qquad (45)$$

would create a potential difference across the open gap of the ring given by

$$\Phi_{ring}(t) = \int_0^{2\pi-\delta} Rd\theta E_\theta(R, \theta, z_0) \simeq -\frac{\mu_0}{4\pi}\int_0^{2\pi-\delta} Rd\theta \int d^3\vec{r}' \frac{\partial_t J_\theta(\vec{r}', t)}{|\vec{r} - \vec{r}'|}. \qquad (46)$$

The quantities $\phi_{ring}(t)$ and $\Phi_{ring}(t)$ represent integration over angular coordinates of both source points and field points and *hence are sensitive only to the symmetric portion of charge density and time derivative of azimuthal current density.* While $\phi_{ring}(t)$ is angular integral over a scalar quantity, $\Phi_{ring}(t)$ is a line integral over a vector quantity. Under the transformation $\theta \to -\theta$, the former is symmetric while the latter is anti-symmetric.

Now consider two identical rings kept close together but connected to coaxial cables in clockwise (CW) and counterclockwise (CCW) sense and connected to two oscilloscope channels with proper impedance matching terminations at both ends. The center conductor of each cable would see a voltage $\phi_{ring}(t)\pm\Phi_{ring}(t)$ while the outer conductor of both would see a voltage $\phi_{ring}(t)$. In other words, the cables would carry a common-mode signal $\phi_{ring}(t)$ and a differential mode signal $\pm\Phi_{ring}(t)$. The differential amplifier of the oscilloscope will then have an output given by

$$\begin{aligned} V_{CW} &= A_{CM}\phi_{ring}(t) + A_D\Phi_{ring}(t); \\ V_{CCW} &= A_{CM}\phi_{ring}(t) - A_D\Phi_{ring}(t), \end{aligned} \qquad (47)$$

where A_{CM} and A_D are common mode and differential mode gain of the oscilloscope input amplifier, respectively.

Define $V_{SYM} \equiv (V_{CW} + V_{CCW})/2 = A_{CM}\phi_{ring}(t); V_{ASYM} \equiv (V_{CW} - V_{CCW})/2 = A_D\Phi_{ring}(t)$.

The experimental signature of the existence of symmetric component of azimuthal current density would be nonzero V_{ASYM}. By virtue of the insensitivity of the integrals (44) and (46) to both source and field angular coordinates, this diagnostic is insensitive to helical perturbations, radial restrike, current filamentation, formation of off-axis plasma structures, and all such non-symmetric plasma phenomena.

The time integration of V_{ASYM} would contain information about the emergence, persistence, and decay of symmetric part of azimuthal vector potential. Since this plays a central role in the creation of a poloidal potential well that is supposed to hold ions within the boundaries of the CK mode for times much longer than the transit time across the plasma, its measurement should yield quantitative data relevant to the refinement of the proposed model.

The significance of this technique and the qualitative model discussed above can be illustrated in reference to an experiment[60] on a 100 J plasma focus where the authors claim "in most of the discharges, it was found that neutrons are originated before HXRs in the axial direction and after HXRs in the radial direction. In some discharges, the time difference between HXRs and neutrons origin was found large enough, so that it can be interpreted that those neutrons would have been originated before the pinch." Clearly, the process of imparting sufficient energy to deuterons to cause reactions cannot involve the conversion of magnetic or kinetic energy associated with the imploding plasma into thermal energy via compression due to stagnation. Also, sufficient path length for accelerated deuterons to cause significant yield exists only in the azimuthal direction. The question of acceleration and trapping of ions into a circular path then occupies the center stage along with the associated questions of its cause and occurrence in time. Fielding this technique would yield conclusive evidence regarding involvement of spontaneously self-organized states in the process of neutron generation in the plasma focus. This also raises the question of a targeted diagnostic for the spatiotemporal correlation between sources of hard x-rays and fusion neutrons.

B. Lateral asymmetry in side-on space-resolved neutron energy spectrum

Space resolved measurements of energy spectrum of fusion protons has been reported only in the Ph.D. thesis of Jaeger[19] and of fusion neutrons only in the conference report from Frascati.[18] This meager data have been ignored by the plasma focus community both because of inaccessibility of these reports and because of absence of follow-up measurements by the respective laboratories. The experimental evidence cited in the Introduction, and the above model proposed to understand it, provides a fresh incentive to resurrect these measurement in a modern version that is amenable to easy replication in multiple laboratories.

The proposed scheme is based on the developments in the technology of GEM detectors[61] based on lithographic etching of thin polyimide sheets. This technology has been successfully utilized to create a matrix of 70 μm diameter holes on a 140 μm pitch in 50 μm thick polyimide sheets with an alignment accuracy of a few micrometers. A stack of such sheets containing such matrix spanning an area of ~10 cm x 10 cm and having a stack thickness equal to the twice the neutron mean free path in polyimide would then act as a *dense array of fast neutron collimators*. This is placed in contact with an acrylic sheet that acts as a fast neutron to fast recoil proton convertor. This is then placed in contact with a thin stack of polyimide matrix sheets that act as *fast recoil proton collimators*. A solid state nuclear track detector (SSNTD) film is placed in contact with this stack. The entire assembly is carefully aligned with the plasma focus so that the central normal to the stack passes through the center of the pinch at 90° to the axis. This assembly shall be referred to as micro-collimator-array-detector (μCAD).

Only neutrons that pass along the aligned holes in the front collimator fall on the recoil proton convertor without losing energy while those that deviate will lose about half their energy in their first collision with a polyimide proton. Only those recoil protons which emerge perpendicular to the convertor will fall on the SSNTD without losing energy after passing through the second collimator stack. The energy of recoil protons incident on the SSNTD therefore is related unambiguously to the energy of the neutrons emitted at 90° to the axis. The tracks on the SSNTD are clustered in the form of a matrix and each cluster can be indexed in a unique manner. The neutron spectrum and fluence of each cluster can be evaluated using standard techniques.[62]

This diagnostic should be sensitive to spatial distribution of fluence and CM energy of reacting deuterons with sub-millimeter spatial resolution. Detection and quantification of lateral asymmetry in these data should act as a probe of existence of circular and toroidal orbits.

C. Complementary radial variation of neutron energy spectrum at 0° and 180°

This diagnostic arrangement is similar to the micro-collimator-array-detector (μCAD) described in Sec. IV B except that there are two identical assemblies and their center normals are aligned with the device axis along 0° and 180°. Again the neutrons which are aligned with the collimator array will create a matrix of track clusters on the SSNTDs. The energy distribution of neutrons and total number of tracks can be determined for each track cluster as in the previous case.

This diagnostic would yield the following information:

1. Symmetry (or lack of it) of track distribution around the center. Such symmetry should exist if the neutron emission is indeed from ions trapped in the poloidal potential well. Conversely, if the neutron emission (or a significant part of it) arises from an off-axis sub-millimeter plasma structure,[51] or a non-symmetric acceleration and trapping mechanism then it should be revealed in the side-on μCAD as well as the two end-on μCADs.
2. If there is symmetry, then it needs to be checked whether corresponding clusters on the two end-on μCADs have spectra that are shifted in opposite (complementary) sense, as would be expected from the poloidal motion of the trapped ions. The shift of the spectral peak is likely to be a function of radial distance of the cluster.
3. The μCAD data can be analyzed to yield estimates of the radial and axial extent of the poloidal potential well so that a quantitative refinement of the suggested model can be attempted.
4. Fluence anisotropy can be determined for voxels in the plasma both as ratios of downstream-to-side-on and upstream-to-side-on cluster-wise fluence. This can serve as a stringent cross-check on any quantitative model of ion acceleration and trapping.

D. Space-time relation between the reaction zone and the magnetic structure

The μCAD described above yields space-resolved, time-integrated information about the neutron spectrum, fluence as well as radial and axial dimensions of the time-integrated neutron source with sub-millimeter spatial resolution. A modification of this can yield coarse-grained spatial structure as a continuous function of time that can be correlated with the diagnostic for azimuthal current density described above. This requires development of GEM (or THGEM) detector stacks working in current mode rather than in counting mode being used at present in particle physics applications. The counting mode operation has a maximum proton incidence rate below which the individual recoil protons can be distinguished as separate signals. The plasma focus application would most probably exceed this limit.

The concept involves a GEM detector stack having many more stages than are required for particle physics applications that replaces the SSNTD in the μCAD. The GEM-stack is equipped with readout electrodes in the shape of concentric rings, with each ring connected to ground of the GEM power supply through a 47 Ohm load resistance. The proton incidence rate would be orders of magnitude larger than the maximum counting rate and the result would be a single pulse across each load resistance, which can be connected to an oscilloscope channel. This assembly is placed at 0° with its center normal aligned with the device axis. The signals then indicate the radial extent of the neutron source as a continuous function of time that can be correlated with the diagnostic with CW and CCW coils outlined above.

Unlike counting mode applications in particle physics, stray breakdowns of the GEM detector stack have no adverse effect on this diagnostic because such breakdowns are not registered on the externally triggered digital storage oscilloscopes. Uniformity of gain across the entire stack, which is a requirement for particle physics, is not a concern since the amplified output is being collected on concentric ring electrodes, whose purpose is to detect the radial extent of the neutron source as a function of time. While conventional GEM stacks

develop the signal across a mega-Ohm load resistance that matches input impedance of the pre-amplifier, the proposed diagnostic needs to have a 47 Ohm load resistance for impedance matching with the coaxial cable. This implies a much larger number of stages in the GEM stack, which needs some development studies.

E. Time-resolved sub-millimeter scale imaging of hard x-rays

The above techniques based on using a current-mode GEM detector stack along with μCAD can in principle be adapted for time resolved sub-millimeter scale imaging of hard x-rays which can be compared with the corresponding neutron image. A *dense array of hard x-ray collimators* can be created by using double-sided copper-clad polyimide laminates with matrix of $70\,\mu m$ diameter holes on a $140\,\mu m$ pitch which is electroplated on both sides with gold (or lead) to a high practical thickness ($1-5\,\mu m$?) and then creating a stack with enough opacity for the desired range of x-ray energy. The fast neutron to recoil proton convertor is replaced with a single-sided copper-clad polyimide sheet without holes coated with gold to serve as x-ray to electron convertor. The resulting fast electron signal is amplified by a current-mode GEM detector stack. The readout can be an array of ionization current collectors.

This system can be operated together with the reaction zone imager described above to investigate the existence or absence of spatiotemporal correlation between the HXR source and reaction zone.

V. SUMMARY AND CONCLUSIONS

This section summarizes and concludes the paper.

The objective of this paper is as follows:

- to summarize available experimental evidence from plasma focus research that suggests that spontaneously self-organized states (SSS) of magneto-plasma play a crucial role in neutron emission from plasma focus,
- to outline a theoretical approach that yields an analytical handle on the likely 3-dimensional structure of the SSS without being hampered by the lack of a close-in metallic boundary and externally controlled magnetic flux required in plasma relaxation theories,
- to construct a qualitative description of ion trajectories in such SSS and compare it with experimental evidence, and
- to suggest a new generation of diagnostic techniques that are sensitive to the qualitative signatures of the resulting narrative and capable of yielding necessary data for refinement of the narrative into a quantitative model.

This effort is inspired by extensive recent work at the PF-1000 facility at the International Center for Dense Magnetized Plasmas in Warsaw that strongly suggests that the early part of neutron emission is caused by fast deuterons with energy on the order of $\sim 100\,keV$, having approximately equal axial and radial velocity, temporally coinciding with the occurrence of self-organized, bounded magneto-plasma structures, which remain trapped within the reaction zone for tens of transit times. Its main motivation is the observation that existing models of plasma focus cannot accommodate 3-dimensional descriptions of magnetic field and ion trajectories within their scope and current theoretical framework dealing with magnetic reconnection/self-organization in plasmas cannot be utilized for the plasma focus case because it requires conducting

boundaries close to the plasma and an externally controlled source of magnetic flux, both of which are absent in the plasma focus case.

Instead, this paper proposes a qualitative "narrative" where plasma dynamics, transformed into cylindrical Fourier space, tends to concentrate spectral amplitude density of solenoidal, scalar, and irrotational fields toward the lower and higher ends of the mode number spectrum with physical limits provided by the plasma size and the microscopic plasma model. Solenoidal fields (such as magnetic field, current density, and vector potential) then acquire the form of a super-position of eigenfunctions of curl, while the scalar fields (density, temperature) acquire the form of a superposition of eigenfunctions of the Laplacian. It is shown that this narrative closely agrees with the qualitative phenomenology of plasma transformations on PF-1000.

With the identification of an analytical form for the structure of magnetic field, it becomes feasible to write the equations of motion for ion trajectories in 3 dimensions. For stationary and symmetric magnetic field, the trajectories have two constants of motion—the canonical angular momentum and total energy. It is shown that the ion motion restricted by these constants of motion is formally equivalent to a two dimensional potential well problem for the (poloidal component of) ion motion in the (r, z) plane. A contour map of the potential function reveals that the ion motion is confined to a toroidal region. Ion trajectories at the bottom of this potential well correspond to circular orbits that theoretically never leave the mode boundaries. Trajectories that have a limited poloidal motion have a residence time that is larger than transit time across the mode. Those whose poloidal energy exceeds a threshold escape the mode. This broad classification of ion trajectories is expected to hold when a particular eigenmode of the magnetic field grows and decays over timescales larger than the Larmor period. For such quasi-stationary modes, canonical angular momentum and energy may vary over time scales much larger than the transit time across the mode. This would be equivalent to a poloidal potential well which changes slowly with time—a kind of adiabatic approximation to the ion motion.

This narrative explains the following non-trivial qualitative features in a unified manner:

- why the neutron emission lasts longer than the ion transit time,
- why it reveals energy isotropy for reacting deuterons,
- why it exhibits signatures of azimuthal motion of center of mass of reacting deuterons,
- why neutrons appear to be emitted perpendicular to the axis in POSEIDON
- why high energy ions are detected in both downstream and upstream axial directions
- why the size of the reaction zone appears to be larger than that of the dense plasma, and
- why a low divergence axial ion beam is often detected in the plasma focus.

A crucial role is played in this effort by experimental results which show existence of an azimuthal component of the center-of-mass velocity of reacting deuterons inferred through space resolved, time-integrated spectroscopy of fusion neutrons and fusion protons.[5,19,20] Unfortunately, these results were reported from laboratories that no longer exist, published only in the form of a Ph.D. dissertation and a conference publication, never followed up by those laboratories and generally ignored by the plasma focus community. This is the major

reason why the present effort is deliberately restricted to a qualitative narrative rather than a predictive numerical model. Until these results are replicated in existing laboratories, a question mark will always hang over any theoretical construct that is consistent with them

To facilitate such replication, this paper proposes five diagnostic schemes that are untried, feasible, and sufficiently sensitive to the proposed narrative that null results from well-designed experiments can falsify the suggested narrative. They also are capable for providing good quality data that can guide construction of quantitative predictive models of neutron emission in the plasma focus.

To conclude, this paper is meant to be the beginning of an investigation into the phenomenon of acceleration and trapping of fast ions in self-organized magneto-plasma structures in the dense plasma focus and not a definitive answer to any of the relevant questions.

ACKNOWLEDGMENTS

REFERENCES

[1]J. W. Mather, "Dense plasma focus," in *Methods of Experimental Physics* (Elsevier, 1971), Vol. 9B, pp. 187–249.

[2]A. Bernard, H. Bruzzone, P. Choi, H. Chuaqui, V. Gribkov, J. Herrera, K. Hirano, S. Lee, C. Luo, F. Mezzetti, M. Sadowski, H. Schmidt, K. Ware, C. S. Wong, and V. Zoita, "Scientific status of the dense plasma focus," J. Moscow Phys. Soc. **8**, 93–170 (1998).

[3]V. A. Gribkov, "Dense plasma focus: Current and perspective applications," *School and Training Course on Dense Magnetized Plasma as a Source of Ionizing Radiations, Their Diagnostics and Applications* (Abdus Salam International Center for Theoretical Physics, Trieste, Italy, 2012).

[4]M. Krishnan, "The dense plasma focus: A versatile dense pinch for diverse applications," IEEE Trans. Plasma Sci. **40**, 3189 (2012).

[5]S. K. H. Auluck, "Axial magnetic field and toroidally streaming fast ions in the dense plasma focus are natural consequences of conservation laws in the curved axisymmetric geometry of the current sheath," Phys. Plasmas **21**, 102515 (2014).

[6]S. K. H. Auluck, "Dense plasma focus: A question in search of answers, a technology in search of applications" Plasma Science and Applications (ICPSA 2013)," Int. J. Mod. Phys.: Conf. Ser. **32**, 1460315 (2014).

[7]G. Bockle, J. Ehrhardt, P. Kirchesch, N. Wenzel, R. Batzner, H. Hinsch, and K. Hübner, "Spatially resolved light scattering diagnostic on plasma focus devices," Plasma Phys. Controlled Fusion **34**, 801–841 (1992).

[8]M. J. Bernstein, D. A. Mescan, and H. L. L. Van Passen, "Space, time and energy distribution of neutrons and x-rays from a focussed plasma discharge," Phys. Fluids **12**, 2193–2202 (1969).

[9]J. H. Lee, L. P. Shomo, M. D. Williams, and H. Hermansdorfer, "Neutron production mechanism in a plasma focus," Phys. Fluids **14**, 2217–2223 (1971).

[10]P. Kubes, J. Kravarik, D. Klir, K. Rezac, M. Scholz, M. Paduch, K. Tomaszewski, I. Ivanova-Stanik, B. Bienkowska, L. Karpinski, M. J. Sadowski, and H. Schmidt, "Correlation of radiation with electron and neutron signals taken in a plasma-focus device," IEEE Trans. Plasma Sci. **34**, 2349–2355 (2006).

[11]C. Maisonnier, C. Gourlan, G. Luzzi, L. Papagno, F. Peccorella, J. P. Rager, B. V. Robouch, and P. Samuelli, "Structure of the dense plasma focus—Part II: Neutron measurements and phenomenological description," Plasma Phys. Controlled Nucl. Fusion **1**, 523–535 (1971).

[12]V. A. Gribkov, A. Banaszak, B. Bienkowska, A. V. Dubrovsky, I. Ivanova-Stanik, L. Jakubowski, L. Karpinski, R. A. Miklaszewski, M. Paduch, M. J.

[13]Sadowski, M. Scholz, A. Szydlowski, and K. Tomaszewski, "Plasma dynamics in the PF-1000 device under full-scale energy storage: II. Fast electron and ion characteristics versus neutron emission parameters and gun optimization perspectives," J. Phys. D: Appl. Phys. **40**, 3592 (2007).

[13]M. J. Bernstein and G. G. Comisar, "Neutron energy and flux distributions from a crossed-field acceleration model of plasma focus and Z-pinch discharges," Phys. Fluids **15**, 700 (1972).

[14]H. Schmidt, A. Kasperczuk, M. Paduch, T. Pisarczyk, M. Scholz, K. Tomaszewski, and A. Szydłowski, "Review of recent experiments with the megajoule PF-1000 plasma focus device," Phys. Scr. **66**, 168–172 (2002).

[15]M. V. Roshan, P. Lee, S. Lee, A. Talebitaher, R. S. Rawat, and S. V. Springham, "Backward high energy ion beams from plasma focus," Phys. Plasmas **16**, 074506 (2009).

[16]H. Schmidt, P. Kubes, M. J. Sadowski, and M. Scholz, "Neutron emission characteristics of pinched dense magnetized plasmas," IEEE Trans. Plasma Sci. **34**, 2363 (2006).

[17]M. M. Milanese and J. O. Pouzo, "Evidence of non-thermal processes in a 1-MJ plasma focus device by analyzing the neutron spectra," Nucl. Fusion **18**, 533–536 (1978).

[18]J. P. Rager, "Progresses on Plasma Focus research at Frascati," in Invited Paper at the 10th European Conference on Plasma Physics and CTR, Frascati Report No. 81.43/cc (1981).

[19]U. Jaeger, Ph.D. thesis (1986).

[20]J. P. Rager, L. E. Bilbao, H. A. Bruzzone, C. Gourlan, U. Guidoni, H. Kroegler, S. Podda, B. V. Robouch, and K. Steinmetz, "Experiments on neutron production phase of Frascati 1-MJ plasma focus (IAEA-CN-38/G-3)," in Proceedings of the 8th International Conference on Plasma Physics and Controlled Fusion, Brussels (1980), p. 209.

[21]V. A. Bahilov, M. G. Belkov, P. A. Belyaev, I. V. Volubev, V. A. Gribkov, A. V. Dubrovsky, V. M. Zaytsev, Y. F. Igonin, A. I. Isakov, N. V. Kalachev, E. D. Korop, O. N. Krokhin, I. S. G. Kuznetsov, Y. V. Marakov, and V. Y. Nikulin, "Experimental investigations on 'PLAMYA' installation," paper presented at the 4th International Workshop on Plasma Focus and Z-Pinch Res., Warsaw, 9–11 September, 1985.

[22]H. Herold, L. Bertalot, K. Hirano, U. Jager, H. J. Kaeppeler, M. Sadowskj1, H. Schmidt, R. Schmidt, M. Shakhatre, A. Shyam, G. Bockle, K. Matl, N. Wenzel, R. Wolf, R. Batzner, H. Hinsch, and K. Hubner, "Two phases of neutron production in the POSEIDON plasma focus," in Proceedings of the International Conference on Plasma Physics and Controlled Nuclear Fusion Research (1984), Vol. 2, p. 579.

[23]U. Jager and H. Herold, "Fast ion kinetics and fusion reaction mechanism in the plasma focus," Nucl. Fusion **27**, 407 (1987).

[24]K. Steinmetz, K. Hubner, J. P. Rager, and B. V. Robouch, "Neutron pinhole camera investigations on temporal and spatial structures of plasma focus neutron source," Nucl. Fusion **22**, 30 (1982).

[25]M. Sadowski, H. Herold, H. Schmidt, and M. Shakhatre, "Filamentary structure of the pinch column in plasma focus discharges," Phys. Lett. **105A**, 117 (1984).

[26]W. H. Bostick, "Experimental study of ionized matter projected across a magnetic field," Phys. Rev. **104**(2), 292–299 (1956).

[27]P. Kubes, M. Paduch, T. Pisarczyk, M. Scholz, T. Chodukowski, D. Klir, J. Kravarik, K. Rezac, I. Ivanova-Stanik, L. Karpinski, M. J. Sadowski, K. Tomaszewski, and E. Zielinska, "Spontaneous transformation in the pinched column of the plasma focus," IEEETPS **39**, 562 (2011).

[28]P. Kubes, M. Paduch, J. Cikhardt, D. Klir, J. Kravarik, K. Rezac, B. Cikhardtova, J. Kortanek, and E. Zielinska, "The evolution of the plasmoidal structure in the pinched column in plasma focus discharge," Plasma Phys. Controlled Fusion **58**, 045005 (2016).

[29]V. I. Krauz, K. N. Mitrofanov, M. Scholz, M. Paduch, P. Kubes, L. Karpinski, and E. Zielinska, "Experimental evidence of existence of the axial magnetic field in a plasma focus," Europhys. Lett. **98**, 45001 (2012).

[30]P. Kubes, V. Krauz, K. Mitrofanov, M. Paduch, M. Scholz, T. Piszarzcyk, T. Chodukowski, Z. Kalinowska, L. Karpinski, D. Klir, J. Kortanek, E. Zielinska, J. Kravarik, and K. Rezac, "Correlation of magnetic probe and neutron signals with interferometry figures on the plasma focus discharge," Plasma Phys. Controlled Fusion **54**, 105023 (2012).

[31]P. Kubes, M. Paduch, T. Pisarczyk, M. Scholz, T. Chodukowski, D. Klir, J. Kravarik, K. Rezac, I. Ivanova-Stanik, L. Karpinski, K. Tomaszewski, and E.

Zieliñska, "Interferometric study of pinch phase in plasma-focus discharge at the time of neutron production," IEEE Trans. Plasma Sci. **37**, 2191 (2009).

[32]P. Kubes, M. Paduch, J. Cikhardt, B. Cikhardtova, D. Klir, J. Kravarik, K. Rezac, E. Zielinska, M. J. Sadowski, A. Szymaszek, K. Tomaszewski, and D. Zaloga, "Transformation of the ordered internal structures during the acceleration of fast charged particles in a dense plasma focus," Phys. Plasmas **24**, 072706 (2017).

[33]P. Kubes, M. Paduch, M. J. Sadowski, J. Cikhardt, B. Cikhardtova, D. Klir, J. Kravarik, V. Munzar, K. Rezac, E. Zielinska, E. Skladnik-Sadowska, A. Szymaszek, K. Tomaszewski, and D. Zaloga, "Characterization of fast deuterons involved in the production of fusion neutrons in a dense plasma focus," Phys. Plasmas **25**, 012712 (2018).

[34]P. Kubes, M. Paduch, M. J. Sadowski, J. Cikhardt, B. Cikhardtova, D. Klir, J. Kravarik, V. Munzar, K. Rezac, E. Skladnik-Sadowska, A. Szymaszek, K. Tomaszewski, D. Załoga, and E. Zieliñska, "Evolution of a pinch column during the acceleration of fast electrons and deuterons in a plasma-focus discharge," IEEE Trans. Plasma Sci. **47**, 339–345 (2019).

[35]P. Kubes, M. Paduch, J. Cikhardt, D. Klir, J. Kravarik, K. Rezac, J. Kortanek, B. Cikhardtova, and E. Zielinska, "Existence of a return direction for plasma escaping from a pinched column in a plasma focus discharge," Phys. Plasmas **22**, 052706 (2015).

[36]P. Kubes, M. Paduch, M. J. Sadowski, J. Cikhardt, B. Cikhardtova, D. Klir, J. Kravarik, R. Kwiatkowski, V. Munzar, K. Rezac, E. Skladnik-Sadowska, A. Szymaszek, K. Tomaszewski, D. Zaloga, and E. Zielinska, "Features of fast deuterons emitted from plasma focus discharges," Phys. Plasmas **26**, 032702 (2019).

[37]E. G. Zweibel and M. Yamada, "Perspectives on magnetic reconnection," Proc. R. Soc. A **472**, 20160479 (2016).

[38]N. F. Loureiro and D. A. Uzdensky, "Magnetic reconnection: From the Sweet-Parker model to stochastic plasmoid chains," Plasma Phys. Controlled Fusion **58**, 014021 (2016).

[39]J. B. Taylor, "Relaxation of toroidal plasma and generation of reverse magnetic fields" Phys. Rev. Lett. **33**, 1139 (1974); "Relaxation and magnetic reconnection in plasmas," Rev. Mod. Phys. **58**, 741 (1986).

[40]R. N. Sudan, "Stability of field-reversed, force-free, plasma equilibria with mass flow," Phys. Rev. Lett. **42**, 1277 (1979).

[41]L. Turner, "Hall effects on magnetic relaxation," IEEE Trans. Plasma Sci. **14**, 849 (1986).

[42]L. C. Steinhauer and A. Ishida, "Relaxation of a two-specie magnetofluid," Phys. Rev. Lett. **79**, 3423 (1997).

[43]Z. Yoshida and S. Mahajan, "Variational principles and self-organization in two-fluid plasmas," Phys. Rev. Lett. **88**, 95001 (2002).

[44]B. Dasgupta, P. Dasgupta, M. S. Janaki, T. Watanabe, and T. Sat, "Relaxed states of a magnetized plasma with minimum dissipation," Phys. Rev. Lett. **81**, 3144 (1998).

[45]I. Khalzov, F. Ebrahimi, D. D. Schnack, and V. V. Mirnov, "Minimum energy states of the plasma pinch in standard and Hall magnetohydrodynamics," Phys. Plasmas **19**, 012111 (2012).

[46]S. Chandrasekhar and P. C. Kendall, "On force-free magnetic fields," Astrophys. J. **126**, 457 (1957).

[47]S. M. Mahajan and M. Lingam, "Multi-fluid systems: Multi-Beltrami relaxed states and their implications," Phys. Plasmas **22**, 092123 (2015).

[48]S. K. H. Auluck, "Coherent effects in the stochastic electrodynamics of two-fluid plasma," e-print (2012).

[49]S. K. H. Auluck, "On the integral of the product of three bessel functions over an infinite domain: Fourier-space representation of nonlinear dynamics of continuous media in cylindrical geometry," Math. J. **14**, 1–29 (2012).

[50]L. Soto, C. Pavez, F. Castillo, F. Veloso, J_e Moreno, and S. K. H. Auluck, "Filamentary structures in dense plasma focus: Current filaments or vortex filaments?," Phys. Plasmas **21**, 072702 (2014).

[51]E. J. Lerner, S. K. Murali, D. Shannon, A. M. Blake, and F. Van Roessel, "Fusion reactions from >150 keV ions in a dense plasma focus plasmoid," Phys. Plasmas **19**, 032704 (2012).

[52]M. J. Sadowski and A. Malinowska, "Formation and role of filaments in high current discharges of the pinch type," Czech. J. Phys. **56**, B364 (2006).

[53]M. J. Sadowski1, M. Paduch, E. Skladnik-Sadowska, W. Surala, D. Zaloga, R. Miklaszewski, E. Zielinska, and K. Tomaszewski, "Soft x-ray studies of plasma-focus pinch structures in PF-1000U experiments," Plasma Sources Sci. Technol. **24**, 055003 (2015).

[54]A. B. Kukushkin, V. A. Rantsev-Kartinov, and A. R. Terentiev, "Self-organization phenomena in dense plasma focus experiments," in *Strongly Coupled Coulomb Systems*, edited by G. J. Kalman, K. B. Blagoev, and J. M. Rommel (Plenum Press, New York, 1998), pp. 129–133.

[55]A. Kukushkin and V. A. Rantsev-Kartinov, "Dense Z-pinch plasma as a dynamical percolating network: From laboratory plasmas to a magnetoplasma universe," Laser Part. Beams **16**(3), 445–471 (1998).

[56]S. K. H. Auluck, "Role of electron-inertia-linked current source terms in the physics of cylindrically symmetric imploding snowplow shocks," Phys. Plasmas **9**, 4488 (2002).

[57]S. K. H. Auluck, "Re-appraisal and extension of the Gratton-Vargas two-dimensional analytical snowplow model of plasma focus evolution in the context of contemporary research," Phys. Plasmas **20**, 112501 (2013).

[58]B. Cikhardtova, P. Kubes, J. Cikhardt, M. Paduch, E. Zielinska, J. Kravarik, K. Rezac, and J. Kortanek, "Evolution of the small ball-like structures in the plasma focus discharge," Nukleonika **61**(2), 155–159 (2016).

[59]R. L. Gullickson and H. L. Sahlin, "Measurements of high-energy deuterons in the plasma-focus device," J. Appl. Phys. **49**, 1099 (1978).

[60]J. Jain, J. Moreno, D. Morales, S. Davis, B. Bora, G. Avaria, M. J. Inestrosa-Izurieta, and L. Soto, "Observation and interpretation of neutron origin prior to hard x rays and pinch in a hundred joules plasma focus device," Laser Part. Beams **35**(4), 656–662 (2017).

[61]F. Sauli, "The gas electron multiplier (GEM): Operating principles and applications," Nucl. Instrum. Methods Phys. Res., Sect. A **805**, 2–24 (2016).

[62]D. Nikezic, B. Milenkovic, and K. N. Yu, "Databank of proton tracks in polyallyldiglycolcarbonate (PADC) solid-state nuclear track detector for neutron energy spectrometry," Nucl. Instrum. Methods Phys. Res., Sect. A **802**, 97–101 (2015).